ELECTRICAL CHARACTERIZATION OF GOLD FUNCTIONALIZED DNA ORIGAMI NANOTUBES

by

Christopher Vinhtroung Buu

A thesis

submitted in partial fulfillment

of the requirements for the degree of

Master of Science in Electrical Engineering

Boise State University

May 2013

BOISE STATE UNIVERSITY GRADUATE COLLEGE

DEFENSE COMMITTEE AND FINAL READING APPROVALS

of the thesis submitted by

Christopher Vinhtruong Buu

Thesis Title: Electrical Characterization of Gold Functionalized DNA Origami Nanotubes

Date of Final Oral Examination: 28 February 2013

The following individuals read and discussed the thesis submitted by student Christopher Vinhtruong Buu, and they evaluated his presentation and response to questions during the final oral examination. They found that the student passed the final oral examination.

William B. Knowlton, Ph.D.	Chair, Supervisory Committee
Wan Kuang, Ph.D.	Co-Chair, Supervisory Committee
Bernard Yurke, Ph.D.	Member, Supervisory Committee
William L. Hughes, Ph.D.	Member, Supervisory Committee

The final reading approval of the thesis was granted by William B. Knowlton, Ph.D., Chair of the Supervisory Committee. The thesis was approved for the Graduate College by John R. Pelton, Ph.D., Dean of the Graduate College.

ACKNOWLEDGEMENTS

There are several people I need to thank for helping make this thesis possible. Most importantly, I would like to thank my family and friends for their love, support, and encouragement, especially my parents and sister. I am also thankful to have the love of my life, Erma, by my side throughout everything.

I would like to thank my advisor Dr. Bill Knowlton, who allowed me to join his research group as an undergraduate student and to continue on as a graduate student (A special thanks goes to Dr. Amy Moll who passed on my resume to Dr. Knowlton in the first place). Dr. Knowlton provided me the opportunity to perform research and provided guidance and encouragement through most of my time at BSU, and I am sincerely thankful for everything. I would also like to express my gratitude to my thesis committee of my co-chair Dr. Wan Kuang, and members Dr. Bernard Yurke and Dr. William Hughes. Their expertise and advice helped to make completing this thesis possible. I would also like to thank Dr. Elton Graunard, Chad Watson, Dr. Paul Davis, Dr. Jeunghoon Lee, and Dr. Natalya Hallstrom for their time and assistance in everything.

There have been a lot of changes to the research group over the years, but I have always had the opportunity to work with the greatest people. It was an honor to work with all past and present members of the Nanoscale Materials and Device Research group. I enjoyed everyone's company and it helped make getting through the tough times easier. I am very appreciative to have worked with Jason Brotherton, Amber Thompson,

Blake Rapp, Lejmarc Snowball, and Nick Schmidt because of the work they contributed to this thesis.

This work was supported in part by DARPA Contract No. N66001-01-C-80345, NIH Grant No. P20 RR016454, NSF IDR No. 1014922, NSF MRI No. 0923541, NSF MRI No. 0521315, NSF CAREER No. 0846415, LSAMP Fellowship HRD-0901996, and ECE Department Graduate Assistantship.

ABSTRACT

Conductivity types (i.e., insulator, semiconductor, and conductor) can be tuned by varying the size of metallic nanoparticles. DNA origami, a molecular self-assembly technique, has promise to programmatically self-assemble nanoparticles (NPs) with nanometer precision. The work presented here demonstrates the programmatic self-assembly of AuNPs on DNA origami nanotubes (NTs). DNA origami NTs were also functionalized with positively charged Au clusters. DNA origami NTs, both bare and functionalized with Au, were electrically characterized using DC current-voltage (DC-IV) measurements. The measurements showed that bare, undecorated DNA NTs behaved as an insulator, whereas linear, ohmic conductivity was observed for Au enhanced Au decorated NTs. Resistances varied between 60 Ω to 8 MΩ after 15 minutes of electroless Au deposition. After SEM imaging, a decrease in resistances was recorded for several Au enhanced AuNP DNA NTs with final resistances ranging from ~48 Ω to ~170 Ω. DNA origami NTs were also conductive with linear, ohmic behavior and resistances in the MΩ range after 9 minutes of Au enhancement. These results show that by functionalizing the DNA origami NT with AuNPs or Au clusters and increasing the size of the Au, a conductive DNA origami NT could be fabricated. Au-functionalized DNA origami NTs with tunable conductivity may have a variety of electronic and optoelectronic device applications.

TABLE OF CONTENTS

LIST OF TABLES

LIST OF FIGURES

LIST OF ABBREVIATIONS

AC-IS	AC impedance spectroscopy
AFM	Atomic Force Microscopy
AuNP	Gold Nanoparticle
DC-IV	DC Current and Voltage
DNA	Deoxyribonucleic acid
EBL	Electron Beam Lithography
FESEM	Field Emission Scanning Electron Microscopy/Microscope
NT	Nanotube
nt	Nucleotides
PMMA	Poly(methyl methacrylate)
QD	Quantum Dot
RCF	Relative Centrifugal Force
SCS	Semiconductor Characterization System
SEM	Scanning Electron Microscopy/Microscope
TEM	Transmission Electron Microscope
UHP	Ultrahigh-Purity

UPW	Ultra-Purified Water

CHAPTER ONE: INTRODUCTION

Deoxyribonucleic acid (DNA) has shown great promise as a scaffolding material for bottom-up fabrication of novel electronic and optoelectronic nanoscale devices [1]. One technique of programmable, self-assembly of nanometer scale structures based on DNA is scaffolded DNA origami [2]. DNA origami is a self-assembly technique that employs short, synthetic oligonucleotides to interact and thereby fold a long, single-stranded DNA into two and three-dimensional shapes with nanoscale resolution [2-16]. DNA origami structures such as a nanotube (NT) could be used as a "nanobreadboard" [2] and functionalized with various nanoparticles (NPs) such as metals, quantum dots, and organic fluorophores periodically or aperiodically [17, 18]. Mathieu *et al.* created the first six helix bundle from DNA using structural DNA nanotechnology [19]. Douglas *et al.* adopted the design by Mathieu *et al.* and synthesized a six-helix bundle using DNA origami, creating a DNA origami NT [4]. DNA origami NTs were functionalized with controlled, periodic placement of quantum dots (QDs) by Bui *et al.* [17] and with Au by Onodera [18]. But before continuing the discussion of DNA origami structures, other DNA-based structures will be examined.

Multistranded DNA structures have been functionalized with various metals including Ag [20-29], Au [21, 27, 28, 30-44], Co [45, 46], Cu [25, 47, 48], Ni [40, 42, 49, 50], Pt [51-53], and Pd [46, 48, 54-61]. Table 1.1 is a comparison of several DNA-templated metal nanowires.

Table 1.1 Comparison of different DNA-templated metal nanowires

Author	Type of DNA	Metal	Metal Growth	Dimensions	Nanowire Resistance	Resistivity
Braun *et al.* [20]	λ-DNA	Ag ions	Reduction solution	100 nm wide, 12 μm long	7 MΩ	N/A
Richter *et al.* [55]	λ-DNA	Pd ions	Reduction solution	50 nm diameter, ~16 μm long	~743 Ω	N/A
Keren *et al.* [31]	λ-DNA	Ag ions	Electroless Au solution	50-100 nm wide, 4+ μm long	~25 Ω	1.5×10^{-7} Ω·m
Harnack *et al.* [32]	calf thymus DNA	Tris(hydroxymethyl)-phosphine-capped gold nanoparticles	GoldEnhance EM	30-40 nm wide, 2 μm long	2.4 kΩ	3×10^{-5} Ω·m
Ongaro *et al.* [33]	calf thymus DNA	4-(dimethylamino) pyridine (DMAP)-modified gold nanoparticles (3.6 nm diam.)	GoldEnhance LM	40 nm wide, 1.25 μm long, 20 nm tall	103 kΩ (network of nanowires)	10^{-4} Ω·m
Gu *et al.* [40]	λ-DNA	Nanoprobes NanoGold (1.4 nm diam.)	Nanoprobes electroless deposition bath	~120 nm wide, 8.5 μm long	2.1 kΩ	2.7×10^{-6} Ω·m
Yan *et al.* [22]	Custom oligonucleotides (4 × 4 tile)	Ag ions	Nanoprobes HQ Silver EM	43 ± 2 nm wide, 5 μm long, 35 ± 2 nm tall	200 Ω	2.4×10^{-6} Ω·m
Liu *et al.* [23]	Custom oligonucleotides (Triple-crossover tiles)	Ag ions	Nanoprobes HQ Silver EM	25 nm diam., 20 μm long	2.35 to 2.82 kΩ	1.4 to 3.2 × 10^{-5} Ω·m
Pearson *et al.* [44]	T-Shaped DNA Origami	Au nanoparticles (5 nm diam.)	Natan's Au Plating Solution	33 nm wide, 195 nm long	2.4 kΩ	6.2×10^{-6} Ω·m

Braun *et al.* created the first DNA-templated nanowire, which consisted of a Ag wire using λ-DNA as a template for targeted deposition and growth of Ag ions [20]. Lambda DNA was bridged and stretched across two Au electrodes using oligonucleotides bound onto the electrodes. The ends of the λ-DNA were complimentary to the bound oligonucleotides on the electrodes. Ag ions were then attached to the DNA and grown using a reduction solution. Two terminal, DC current and voltage (DC-IV) electrical measurements showed the Ag wires were conductive but a zero bias plateau where there was little conduction was observed. Ohmic behavior was observed in the Ag wires after applying a voltage greater than 50 V on wires with extensive Ag deposition with resistances of 7 MΩ. Others have created nanowires in a manner similar to Braun *et al.*, such as Richter *et al.* who created a conductive nanowire with ohmic behavior using λ-DNA as a template to create Pd nanowires [54]. Lambda DNA strands were aligned across interdigitated Au electrodes using capillary forces by removing a drop of DNA solution perpendicular to the electrodes and the DNA was metallized with Pd afterwards. Extra NTs were removed by cutting the nanowires using a standard micromanipulator with etched, tungsten tips until only one NT remained on the electrode structure. The remaining NT was fixed onto the structure with deposition of electron beam induced carbon lines deposited over the end of the NT. Ohmic behavior was observed in the nanowire with a resistance of 743 Ω. The work by Braun *et al.* and Richter *et al.* demonstrated that DNA could be used as a template to create conductive nanowires.

Other types of DNA have been used as templates for synthesizing and electrically characterizing Au nanowires by several groups. Keren *et al.* used the RecA protein to selectively metallize a DNA substrate using Ag ions and Au electroless plating solution

and created a DNA Au wire that exhibited a resistance of ~25 Ω [31]. Harnack *et al.* used electroless plating of negatively charged tris(hydroxymethyl)-phosphine-capped AuNPs onto calf thymus DNA to create a network of Au nanowires and derived a single wire resistance of 2.4 kΩ [32]. Ongaro *et al.* created Au nanowires using double stranded calf thymus DNA as a template and AuNPs were modified to selectively bind randomly only to the DNA after it had been deposited on interdigitated Au electrodes [33]. The AuNPs attached onto the DNA because the 4-(dimethylamino) pyridine-modified AuNPs are positively charged and the DNA is inherently negatively charged. Continuous nanowires were formed using an electroless deposition of Au. A network of Au nanowires was electrically measured and showed linear, ohmic behavior with an overall resistance of 103 kΩ. Gu *et al.* created Au nanowire structures using λ-DNA as a template and positively charged Au ions as a seeding metal followed by an electroless deposition bath to enlarge the Au [40]. The measured resistance of the Au nanowire was 2.1 kΩ. Aherne *et al.* also created Au nanowires using electroless plating and double stranded calf thymus DNA as a template to perform reliability measurements and examine the failure current density as function of diameter [35]. These Au nanowires are some examples of how different types of DNA other than λ-DNA can also be used as a template for creating conductive structures.

Multistranded DNA structures such as tiles and DNA origami have also been metallized and several were electrically characterized. Yan *et al.* synthesized conductive nanowires using a four-armed structure to create nanoribbons that were metallized with Ag using a two-step procedure of seeding and plating [22]. The resistance of the Ag nanoribbon was 200 Ω and was ohmic in behavior. Liu *et al.* created DNA NTs using

triple-crossover tiles as a basic building block and metallized the structure with AuNPs as a seed and plated with Ag [23]. Electrical conductivity measurements showed linear, ohmic behavior with a resistance of ~2.8 kΩ. Liu *et al.* used a branched DNA origami structure as a template for seeding with AgNPs and electroless plating with Au [43]. Geng *et al.* used a similar branched DNA origami structure as Liu *et al.* and seeded it with Pd and plated the Pd with Au [61]. Pilo-Pais *et al.* demonstrated programmed placement of AuNPs on a "tall rectangle" DNA origami structure and enlarged the AuNPs by reducing silver ions from solution [28]. The DNA origami structure had specific binding sites with unique, DNA strand sequences extending from the structure and the AuNPs were functionalized with the complementary DNA sequence. Schreiber *et al.* used positively charged Au clusters to metallize several different DNA origami structures such as NTs and donuts [42]. Recently, Pearson *et al.* functionalized a "T" shaped DNA origami structure similar to Liu *et al.* [43] and Geng *et al.* [61] with AuNPs, used an electroless plating solution to grow the AuNPs, and electrically characterized the metallized DNA origami [44]. The top of the “T” was decorated with AuNPs using staple strands extending from the top of the T structure to attach to the AuNPs (nominally 5 nm diameter) coated with complementary strands. The AuNP structures are about 195 nm long with an average of 16 AuNPs attached with a center to center spacing of 11.7 nm. A Au electroless plating method was used to grow the AuNPs to create a conductive structure. Electrodes were then written onto a SiO_2 surface using electron beam lithography (EBL) to create a connection to the DNA origami nanowires that were already on the surface for electrical characterization. Direct current and voltage

measurements were performed and the average resistance of the structures was 2.3 kΩ with a standard deviation of 0.6 kΩ.

The metallization and electrical characterization of DNA origami structures is important because it indicates it is possible to create a nanostructure using DNA origami as a substrate. The programmed, site-specific placement of NPs allows one to control the position of the NPs, and the electroless plating/enhancement can be used to increase the size of a NP. Combining the idea of programmed placement of NPs on a DNA origami structure with the electroless plating/enhancement to create a conductive structure could allow one to create a DNA origami device with tunable conductivity by changing the number or size of the NPs.

The actual use of decorated DNA nanostructures as devices is complicated by the question of placing the nanostructures onto electrical contacts. Several groups have demonstrated methods of site-specific placement of synthesized DNA structures with and without subsequent electrical characterization. Kuzyk *et al.* demonstrated dielectrophoretic trapping of a single "smiley face" and triangular DNA origami structures that are approximately 100 nm x 100 nm between two Au electrodes with a 70-90 nm gap. An AC field and thiol linkers on the DNA origami structures were used to help immobilize the structures using thiol-Au covalent bonding [62]. However, the technique did have some challenges as multiple DNA origami structures were observed trapping along the length of the electrodes if the AC voltage and frequency were not optimal [62]. Bellido *et al.* positioned triangular DNA origami structures between two Pt electrodes with a 100 nm gap using an electric field and performed temperature dependent (80K to 360K) DC-IV measurements [63]. It was observed that below 240 K,

the triangular DNA origami has a high impedance and, from temperatures between 280 K to 320 K, the main conduction mechanism is hopping conduction [63]. Bobadilla *et al.* performed AC impedance spectroscopy (AC-IS) measurements using the same Pt electrode structure and triangular DNA origami as Bellido *et al.* [63, 64]. The triangular DNA origami structures were positioned across the gap using a 2 V_{pp} AC voltage. AC impedance spectroscopy measurements of the triangular DNA origami structure showed that the impedance of the structure decreases above 100 kHz and behaves more as a resistor, indicating that it may be possible to transmit signals with frequencies above 100 kHz though the triangular DNA origami structure. DC-IV measurements described in both articles [63, 64] indicated that the triangular DNA origami structure has a high resistance, with Bobadilla *et al.* reporting a resistance of ~20 GΩ, showing the triangular DNA origami electrically acts as an insulator [64]. Linko *et al.* demonstrated dielectrophoretic trapping of a rectangular DNA origami structure using the same technique as Kuzyk *et al.* [62] and performed both DC-IV and AC-IS measurements to determine processes contributing to the DC and AC conductivity [65]. An equivalent-circuit-model was constructed to describe the DC and AC conduction mechanisms, demonstrating that the rectangular DNA origami structure has a low conductivity. Thus, it could be used in the construction of an electrical device if a nonconductive substrate is desired. Linko *et al.* also used dielectrophoresis to trap a streptavidin-decorated DNA triple crossover structure between thiol linker-decorated Au nanoelectrodes [66]. AC impedance spectroscopy measurements showed that the conductivity of the tiles was negligible suggesting that it also could be a suitable scaffold for building an electrical device. Other methods of positioning and orienting DNA origami include lithographically

patterned surfaces for controlled placement of DNA origami triangles [67] and connecting surface patterned Au islands using DNA origami nanotubes modified with thiols [68]. Each of the described methods could provide a method that could allow one to interface DNA nanostructures to electrical contacts for electrical characterization.

Though a DNA origami structure metallized with AuNPs has been synthesized and electrically characterized, a DNA origami NT functionalized with site-specific AuNPs has not been electrically characterized. Also, a DNA origami NT functionalized with Au seeds also has not been electrically characterized. DNA origami NTs would be well suited as a template for a potential Au nanowire because the NT is linear in nature. Changing the size of the Au on a DNA origami NT could allow one to create an electrically conductive structure. DNA origami NTs with tunable conductivity could lead to the fabrication of novel electronic and optoelectronic nanoscale devices. It may also allow further study on the basic physics of one-dimensional metal-insulator transitions [69].

In this thesis, DNA origami NTs periodically functionalized with AuNPs and seeded with positively charged Au clusters were electrically characterized. Chapter 2 describes the materials and methods used to perform the experiments for this thesis. A Au electrode structure was fabricated for interfacing the DNA origami NTs with electrical test instruments for electrical characterization. DNA origami NTs functionalized with both AuNPs and seeded with positively charged Au clusters were bridged across the electrode structures. Gold enhancement was performed to grow the Au and create conductive NTs. Electrical characterization of the DNA origami NTs were performed using DC-IV measurements. Chapter 3 reports the results of the electrical

characterization. It was shown that bare DNA origami NTs were insulators and Au enhanced Au functionalized DNA origami NTs behaved as conductors. Chapter 4 presents a discussion of the results regarding the design of the electrode structures and the measured resistances of the NTs. Chapter 5 provides a conclusion of the work presented in this thesis.

CHAPTER TWO: EXPERMIMENTAL

2.1 Experimental Approach

DNA origami NTs with adjustable numbers of binding sites for NPs and the size of the NPs or Au clusters on a DNA origami NT could allow one to control the electrical behavior of functionalized DNA origami NTs. To test this hypothesis, DNA origami NTs with specific binding sites were synthesized, functionalized with AuNPs or Au seeded with Au clusters, and Au enhanced. The NTs were then deposited onto electrode structures fabricated for interfacing the DNA NTs with electrical characterization instrumentation. Bare DNA origami NTs were electrically characterized to determine if the bare DNA origami NTs can act as a suitable substrate for creating a nanowire. The NTs were functionalized with AuNPs and/or positively charged Au clusters to create a potentially conductive structure. Gold enhancement solution was used to enhance the electrical response of the devices by increasing the size of the AuNPs and Au clusters. Atomic Force Microscopy (AFM) was used to image the synthesized NTs, verify depositions of the NTs onto the electrode structures, and remove debris between the Au electrodes. Scanning Electron Microscopy (SEM) was used to examine and determine the dimensions of the Au enhanced NTs. Transmission Electron Microscopy (TEM) was also used to examine the AuNP functionalized NTs. Electrical characterization was performed using DC current-voltage (DC-IV) measurements to establish whether the nanostructures were conductors, semiconductors, or nonconductors.

2.2 Methods and Materials

2.2.1 DNA Origami Nanotubes

The DNA origami NTs were synthesized using an M13mp18 singled-stranded, viral DNA, which acts as the scaffold strand (New England Biolabs), and 168 unique, synthetic oligonucleotides as the staple strands (Integrated DNA Technologies) to synthesize a six-helix NT bundle [2, 10, 17]. The NTs are designed to be approximately 412 nm in length and 6 nm in diameter. To form the NTs, the M13mp18 viral DNA (~52.5 nM) and the 168 staple strands (each strand solution was ~100 µM) were mixed in a 1:10 molar ratio in a solution of 1x TAE Mg^{++} (40 mM tris, 20 mM acetic acid, 2 mM) ethylene-diaminetetracetic acid (EDTA) and 12.5 mM magnesium acetate; pH 8.0). The solution was thermally annealed at 90 °C for 20 minutes and cooled to 20 °C in steps of 0.1 °C every 10 seconds using a thermocycler (Eppendorf Mastercycler Personal). Following the annealing process, excess staple strands and DNA fragments were filtered using a centrifugal filter (Amicon Ultra 0.5 mL) at 14,000 relative centrifugal force (RCF) for 10 minutes (Eppendorf Centrifuge 5418) and recovered at 1000 RCF for 3 minutes. RCF is calculated using the expression:

$$\mathrm{RCF} = 11.18 \times \mathrm{r} \times \left(\frac{\mathrm{Q}}{1000}\right)^2 \tag{2.1}$$

where r is the distance in cm from the center of the centrifuge rotor to the end of the test tube carrier and Q is the speed of rotation in RPM [70].

2.2.2 Attachment of AuNPs on the DNA Origami Nanotubes

The DNA origami NTs are designed with periodically spaced, DNA linker strands extending from the NT to create binding sites for attaching AuNPs. The DNA origami NTs are designed with 5, 9, 15, and 29 evenly spaced binding sites, resulting in 71 nm, 43 nm, 29 nm, and 15 nm spacing, respectively [17]. AuNPs with a nominal diameter of 5 nm (synthesized by the Department of Chemistry and Biochemistry at Boise State University [18]) were attached onto the DNA origami NT at the different binding sites using complementary DNA linker strands conjugated on the surface of the AuNPs via a thiol linker on the AuNPs that attached to the NT using Watson-Crick base pairing. To attach the AuNPs to the NTs, AuNPs were placed in solution with NTs using a 2:1 ratio of AuNPs to binding sites (i.e., for a NT with 9 binding sites, the ratio of AuNPs to one NT would be 18:1). The 29-site DNA Origami NTs were used for this study because the 29-site DNA origami NTs were designed with an alternating ABC binding site design where A, B, and C are each unique DNA linker strands with corresponding AuNPs to maximize AuNP attachment. The solution was annealed at 50 °C for two hours using a thermocycler (Eppendorf Mastercycler Personal) and filtered by gel electrophoresis in a 0.7% Agarose gel ran at 65V for 2 hours (electrical current ~ 90 mA, gel length is 10 cm) to remove excess AuNPs. AuNP decorated DNA origami NTs were imaged using AFM to ensure valid formation. Transmission Electron Microscopy (TEM) was also used to examine the AuNP functionalized NTs. For this thesis, all 29-site AuNP DNA Origami NTs will be referred to as AuNP DNA NTs.

2.2.3 Metallization of DNA Origami Nanotubes

In addition to AuNP DNA NT functionalization, Au seeding of DNA NTs was used as a strategy to change the conductivity of the DNA origami NTs. In this approach, the DNA origami NTs were metallized using a positively charged Au cluster solution (Nanoprobes Positively Charged NanoGold) [42]. The Au clusters are 1.4 nm in diameter and are coated with positively charged amines that attach to the inherently negatively charged DNA origami NTs. At room temperature, 0.5 µL of 300 µM NanoGold solution was added to 36 µL of 2 nM DNA origami NTs and mixed with a digital vortex mixer (Fisher Scientific Digital Vortex Mixer) for ~30 seconds to 1 minute. After mixing, the Au seeded DNA NT solution was allowed to react overnight. AFM was used to examine the DNA NTs to determine if the positively charged Au clusters seeded the NTs.

2.2.4 Au Enhancement of AuNPs and Au Clusters

To help reduce the distance between the AuNPs on the NT and to increase the size of the Au clusters in an effort to increase conduction, AuNPs and Au clusters were enlarged using a commercial Au electroless plating solution to deposit Au ions (Nanoprobes GoldEnhance EM) [71]. The Au enhancement was performed after the Au decorated DNA origami NTs were deposited on the electrode structure. Four solutions were included with the GoldEnhance EM kit: Solution A (enhancer), Solution B (activator), Solution C (initiator), and Solution D (buffer). 5 µL of Solution A (enhancer) were combined with 5 µL of Solution B (activator). After waiting for 5 minutes, 5 µL of Solution C (initiator) was added to the original solution and deposited on the electrode structure with AuNP decorated DNA origami NTs deposited. Solution D (buffer) was not used to avoid unnecessary dilution of the NT solution. For Au enhancements on the

surface of the wafers of the electrode structures, dilution of the NT solution is not a concern, but for consistency with past Au enhancements in which Solution D was not used, Solution D was not used for this procedure as well. The solution was prepared immediately before use. The AuNPs were then enhanced for 15 minutes and rinsed with 2000 µL of ultra-purified water (UPW). AFM and SEM were subsequently performed to examine the outcome of the Au enhancement. The same Au enhancement method was used for the Au seeded NTs deposited on the electrode structures but were Au enhanced for various amounts of time. The Au seeded NTs were initially Au enhanced for 5 minutes, and an additional 2 minutes of Au enhancement were performed for a total Au enhancement time of 7 and 9 minutes.

2.2.5 Electrode Structure Fabrication

Electrode structures were fabricated to help interface the DNA origami NTs with electrical characterization equipment. Electrode structures were fabricated by electron beam lithography (EBL), DC sputter deposition of both Cr and Au films, and a subsequent lift-off process (see APPENDIX A for more details). The substrates used were 500 µm thick, p-type Si wafers with a 500 nm thick thermally grown SiO_2 (University Wafer). The parallel electrodes were designed to be 1 µm wide and approximately 15 µm in length. The electrodes are lengthened to increase the possibility of NTs bridging the electrodes. The electrodes consisted of a 30 nm Cr adhesion layer and a subsequent 50 nm Au layer. The gap between the parallel finger electrodes was designed to be approximately 250 nm, increasing the probability for the ~400 nm long NT to bridge the electrodes. The 40 µm x 40 µm contact pads allow electrical probe tips with a radius of 1.5 µm to electrically contact the device. Structures were cleaned before

NT depositions using a CO_2 snow clean, a cleaning method that uses a stream of CO_2 and small solid (dry ice) and liquid particles ("snow") to remove particulates off the surface through interactions between the "snow" and contaminates [72]. After the CO_2 clean, structures are rinsed with acetone, isopropanol, and methanol.

2.2.6 DNA Origami Nanotube Deposition

DNA origami NTs were deposited on the electrode structures by pipetting 2 µL of DNA origami NT solution over the electrode structures. A deposition of 10 µL of TAE Ni^{++} buffer solution is then added to the original DNA origami droplet to allow the negatively charged DNA origami to adhere to the potentially negatively charged surface. The droplet is pipette-mixed by aspirating and expelling the droplet five times and allowed to remain on the structure for approximately 10 minutes to facilitate adhesion of the DNA origami NTs to the surface. The electrode structures are rinsed with 2000 µL of UPW to remove any salt precipitates and dried with ultrahigh-purity (UHP) nitrogen gas. To determine if NTs bridged the electrode gap, AFM imaging was performed on the electrode structure.

2.2.7 AFM Imaging and Manipulation, SEM Imaging, and TEM Imaging

AFM was used to verify the formation of the NTs, to determine if NTs were bridging the electrode gap, and to move unwanted debris and NTs from around the gap following DNA NT depositions. AFM images were acquired using the Bruker Dimension Icon FastScan system using a "non-contact" tapping mode. The tip tuned to the attractive side of the tuning curve (APPENDIX B.1) with Si cantilever-based tips (Bruker FastScan-A). Nanoscale manipulation to remove unwanted debris and NTs was

performed with the Bruker Dimension Icon FastScan system using NanoMan. NanoMan is a nanomanipulation and nanolithography technique, with the same FastScan-A tips used for imaging (see APPENDIX B.2). To examine the effects of both Au seeding and AuNP enhancement on a larger sample size of NTs, AFM samples of DNA NTs were prepared by pipetting 1 µL of DNA NT solution onto freshly cleaved mica (V-4) followed by 5 µL of 1x TAE Mg^{++} buffer solution, which was allowed to absorb onto the mica surface for 5 minutes. The mica surface was rinsed with UPW and dried with UHP nitrogen. No additional preparations were performed on electrode structures (with or without NTs) for AFM. SEM images of the Au enhanced DNA origami NTs on the parallel electrode structures were obtained using a Hitachi 4500 field emission scanning electron microscope (FESEM). TEM images of the Au DNA NTs were obtained using a JEOL JEM-2100 HR Analytical Transmission Electron Microscope (TEM) with sample preparation similar to Schreiber *et al.* [42].

2.2.8 Electrical Characterization

After the NTs had been deposited onto the electrode structures and were verified using AFM as bridging the electrodes, DC-IV electrical characterization of the NTs was performed. Bare DNA NTs, AuNP-decorated, and Au seeded DNA NTs were electrically measured. Two terminal, DC-IV measurements were performed using a Keithley 4200 Semiconductor Characterization System (SCS) with source measuring units (SMU) at room temperature. To limit noise from spurious electromagnetic signals, the electrodes with deposited NTs were placed in a Faraday cage during the DC-IV measurements. The voltage was swept from -1 mV to 1 mV and reversed from 1 mV to -1 mV and current was measured simultaneously. The current resolution of the

Keithley 4200 SCS is ~0.1 fA and a 10 µV step size was used. A current compliance of 1 mA was set and an appropriate current range for the SMU was set depending on what current was recorded. Cascade Microtech DCP-115R probe holders and probes were used to interface with the electrode structures on a Micromanipulator probe station.

CHAPTER THREE: RESULTS

3.1 DNA Origami Nanotubes

DNA origami NTs were synthesized and functionalized with AuNPs and Au clusters to create conductive structures. To improve the synthesis and functionalization processes, several imaging techniques were used to characterize the bare and functionalized DNA origami NTs, including AFM, SEM, and TEM. Figure 3.1a shows an AFM height image of a DNA origami NT with AuNPs attached. The design includes a total of 29 binding sites for AuNPs, but only 18 are shown attached to the NT in the figure. An estimated attachment yield of ~55-58% was observed from a sample size of 10 NTs. Despite the low attachment yield, the number of AuNPs attached was greater than the maximum number of AuNPs possible on the other NT designs such as the 9-site or 15-site NTs [18]. Figure 3.1b is the cross section of the height data along the length of the AuNPs decorated NT shown in Figure 3.1a, including measured peak-to-peak spacing between the AuNPs. It is observed that the AuNPs of the NT shown in Figure 3.1a vary in height from ~5 nm to ~9 nm with an average height of ~6.8 nm (i.e. for the 17 of 18 AuNPs shown in the cross section) while the peak-to peak spacing ranges from ~11 nm to ~32 nm with an average spacing of ~20 nm. The nominal diameter of the AuNPs is 5 nm and the expected periodicity of a DNA NT with 29 AuNPs attached is 15 nm, but due to the low attachment yield of AuNPs, the periodicity has increased. The cross sectional height measurement shown in Figure 3.1c is taken along the dotted white line in Figure 3.1a. It shows that the height of the NT is ~2 nm and that the AuNP is ~9 nm. The

designed height of the NT is 6 nm, but Bui *et al.* reported reduced heights for the DNA origami NTs measured using AFM. Possible causes include van der Waals forces collapsing the NT on the surface, compressive forces during AFM imaging, and capillary effects when imaging in ambient conditions [17].

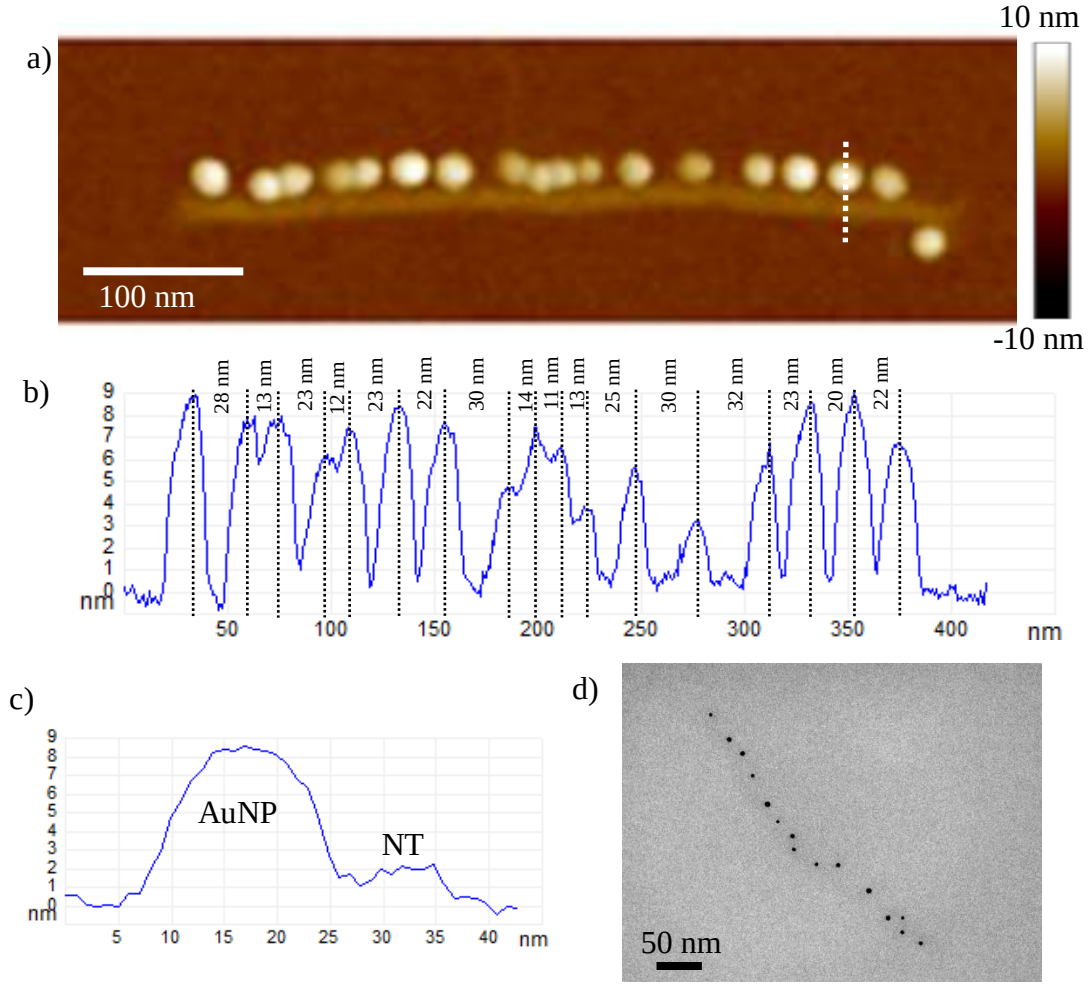

Figure 3.1 (a) AFM height image of a 29-site AuNP origami DNA NT. Only 18 AuNPs are attached onto the imaged NT. (b) Cross sectional AFM height data of 17 of the 18 AuNPs on the NT shown in Figure 3.1a along its length with the measured peak-to-peak spacing between the AuNPs. The average height of the 17 AuNPs is ~6.8 nm. (c) AFM height cross section of white dashed line shown in Figure 3.1a of the AuNP DNA NT comparing the height of the AuNP and DNA NT (d) TEM image of a 29-site DNA origami NT. The average diameter of the AuNPs is ~4.6 nm.

Figure 3.1d is a TEM image of a DNA origami NT decorated with AuNPs. From the TEM image, the diameter of the AuNPs could be determined with an average diameter of 4.6 nm. Using the average diameter of the AuNPs measured from the TEM data (~4.6 nm) and the average height of the AuNPs from the AFM data (~6.8 nm), it appears that the AuNPs are aspherical. It can be assumed that the slight difference between the average AFM height and TEM diameter may be due to the complementary DNA linker strands conjugated via a thiol linker on the AuNPs. The DNA linker strands would appear in the AFM data as the linker strands would add to the overall height of the AuNPs while the DNA linkers would not appear in the TEM data since the contrast between the AuNP and DNA is significant and the AuNPs can be clearly resolved from the DNA.

Positively charged Au clusters were used as an alternative method to functionalize the DNA NTs. Figure 3.2a is an AFM height image of a bare DNA origami NT and Figure 3.2b is the corresponding cross section. The height of the bare DNA NT shown in Figure 3.2a is ~1.5 nm tall. Note that the measured height of the bare NT is also smaller than the designed NT height of 6 nm. Figure 3.2c shows an AFM height image of a DNA origami NT seeded with positively charged Au clusters. The AFM height images obtained in Figure 3.2 were imaged using the same imaging mode and similar scanning parameters. The Au clusters appear to cover the entire surface of the DNA NT. The Au seeded DNA NT is ~9 nm in height when measured in a cross section shown in Figure 3.2d, which is 7.5 nm greater than the 1.5 nm height of the bare NT. The AFM images shown in Figure 3.2 are not of the same NT but representative of the DNA NTs that have been measured. The data shows that the positively charged Au clusters are a possible

alternative method of functionalizing the DNA NTs to create electrically conductive structures.

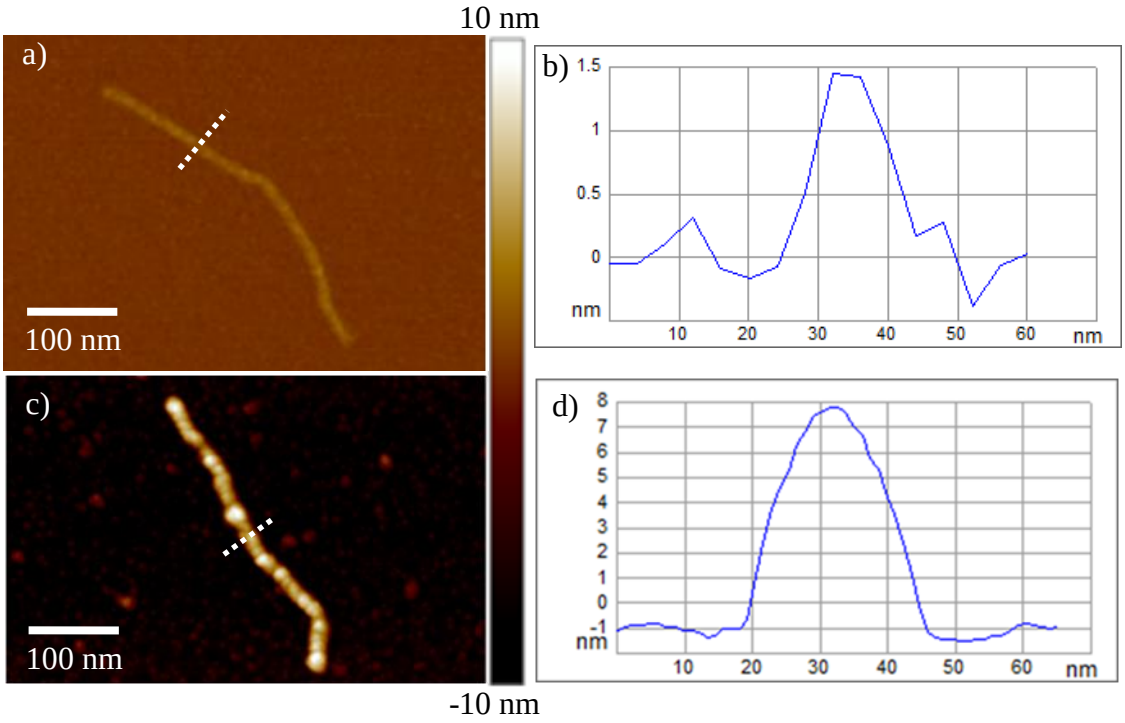

Figure 3.2 (a) AFM height image of bare DNA origami NT. (b) Height cross section along white dotted line in Figure 3.2a. The bare DNA origami NT is ~1.5 nm in height. (c) AFM height image of a DNA origami NT seeded with positively charged Au clusters. (d) Height cross section along the white dotted line in Figure 3.2c. The Au seeded DNA origami NT is ~9 nm in height. The NTs imaged are not the same NT but both NTs are representative of the NTs that have been measured.

3.2 Au Enhancement of DNA Origami Nanotubes

The AuNP functionalized and Au seeded DNA origami NTs were subjected to a Au electroless plating solution to enhance the electrical response. The Au enhanced AuNPs on the NTs are not uniform as denoted by the variations in the height and widths between the NTs, therefore it is difficult to characterize the growth of the AuNPs. Characterization of the height of the 29-site AuNP DNA NTs enhanced for 5, 7, 10, 15, and 20 minutes on both mica and SiO_2 substrates was performed on one set of samples. These experiments were performed to estimate the Au enhancement rate. SiO_2 substrates were chosen to measure the heights of the Au enhanced NTs because (1) the electrode structures were fabricated on SiO_2 wafers and (2) the Au enhancement of the Au DNA NTs were performed on the electrode structures after a DNA NT had bridged the electrodes. Mica was also used because it was believed the SiO_2 surfaces were rougher than the mica, which could cause variations in measured height of the Au enhanced AuNP DNA NTs. Each sample was imaged using AFM and a 3.3 μm × 3.3 μm image was captured. The sample size varied for each measurement but a minimum of 5 AuNP DNA NTs were measured on each sample. The height of several segments (at least 7 segments) of each AuNP DNA NT was measured using AFM and the highest point of each NT was recorded. The maximum heights were then averaged and a standard deviation was calculated. The mean and standard deviation for each sample are given in Table 3.1. The heights measured on both the SiO_2 and mica substrates appear to be similar. The approximate rate of Au enhancement was calculated from a linear fit of the data from Table 3.1. The Au enhancement rate was found to be about 4.61 nm per minute

on SiO_2 (coefficient of determination, R^2=0.979) and 3.71 nm per minute on mica (R^2=0.95).

Table 3.1 Max AuNP height measured and standard deviation

Surface	0 min	5 min	7 min	10 min	15 min	20 min
Mica	9.1 nm (±0.48 nm)	23.1nm (±2.3 nm)	42.8 nm (±8.1 nm)	48.8 nm (±5.1 nm)	73.5 nm (±10.2 nm)	103.3 nm (±18.9 nm)
SiO_2	10.9 nm (±0.38 nm)	29 nm (±4.1 nm)	40.5 nm (±3.4 nm)	65.8 nm (±6.2 nm)	86.3 nm (±9.7 nm)	100.5 nm (±14.5 nm)

AFM and SEM images of the Au enhanced AuNP DNA NTs indicate a non-uniform growth of the AuNPs. AFM data can be used to measure the height of the Au enhanced AuNP DNA NTs to within 0.05 nm but the AuNP width can only be measured to within the AFM tip radius (~ 5nm). However, SEM images will not have AFM tip limitations such as convolution caused by the radius size of the tip, thus SEM can provide a more accurate representation of the width of the Au enhanced NTs. The Au enhanced AuNPs on the NTs varies in height as shown in AFM height image of Figure 3.3a. Figure 3.3b is an SEM image that also confirms the non-uniform variation in width of the Au enhanced AuNP DNA NT. The NTs shown in Figure 3.3a and b were both Au enhanced for 15 minutes. While they are not the same NT, they are from the same NT solution. The Au enhancement also varies from NT to NT as shown in the AFM height image Figure 3.3c.

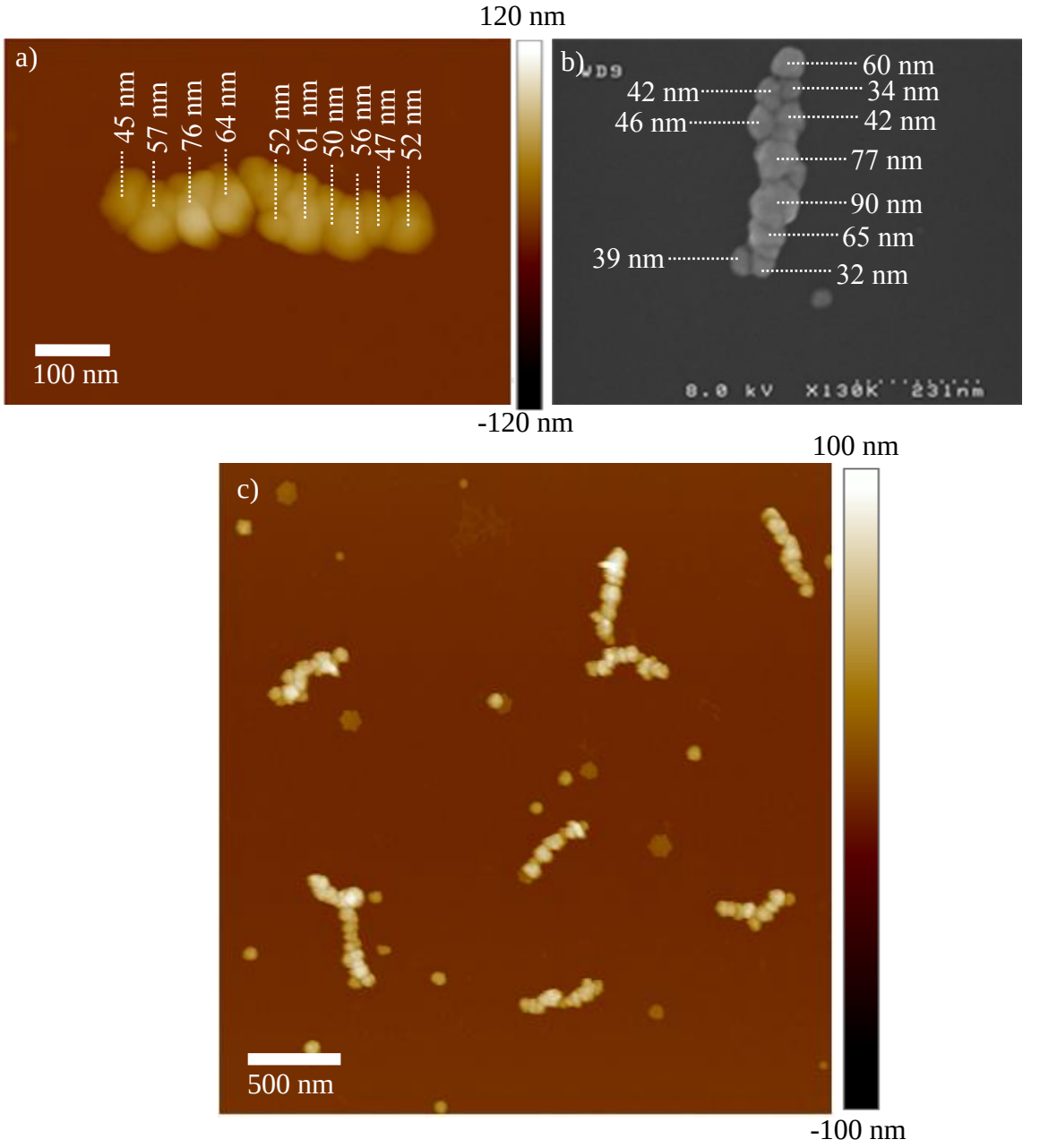

Figure 3.3 (a) AFM height image of AuNP decorated DNA NT Au enhanced on mica for 15 minutes. The height of different segments of the NT is shown. (b) SEM image of AuNP decorated DNA NT Au enhanced for on a Si wafer for 15 minutes. The two NTs shown in this figure are not the same NT. The width of different segments of the NT is shown. (c) AFM height image of AuNP DNA NTs Au enhanced for 15 minutes on SiO2. The Au enhancement also varies from NT to NT as each NT varies in width and height by several nanometers.

3.3 Parallel Electrode Structure

The parallel electrode structure shown in Figure 3.4 had the highest probability of successful bridging of NTs owing to its longer electrodes. Hence, it was chosen as the electrode structure to provide electrical contact to the NTs to perform electrical measurements. Figure 3.4a is an optical micrograph of a successfully fabricated parallel electrode structure. The Au contact pads for the electrical probes are approximately 40 µm x 40 µm to accommodate the electrical probe tips. A magnified view of the Au finger electrodes can be seen in the AFM height image shown in Figure 3.4b, which was used to assess the uniformity of the width and length of the fingers and the gap between the electrode fingers. The parallel finger electrodes are ~1 µm wide and ~15 µm long. Figure 3.4c is a cross section of the Au electrode fingers. The gap between the Au electrodes is ~250 nm and the Au electrodes are ~50 nm tall, creating a suitable area for the NTs to bridge the electrodes.

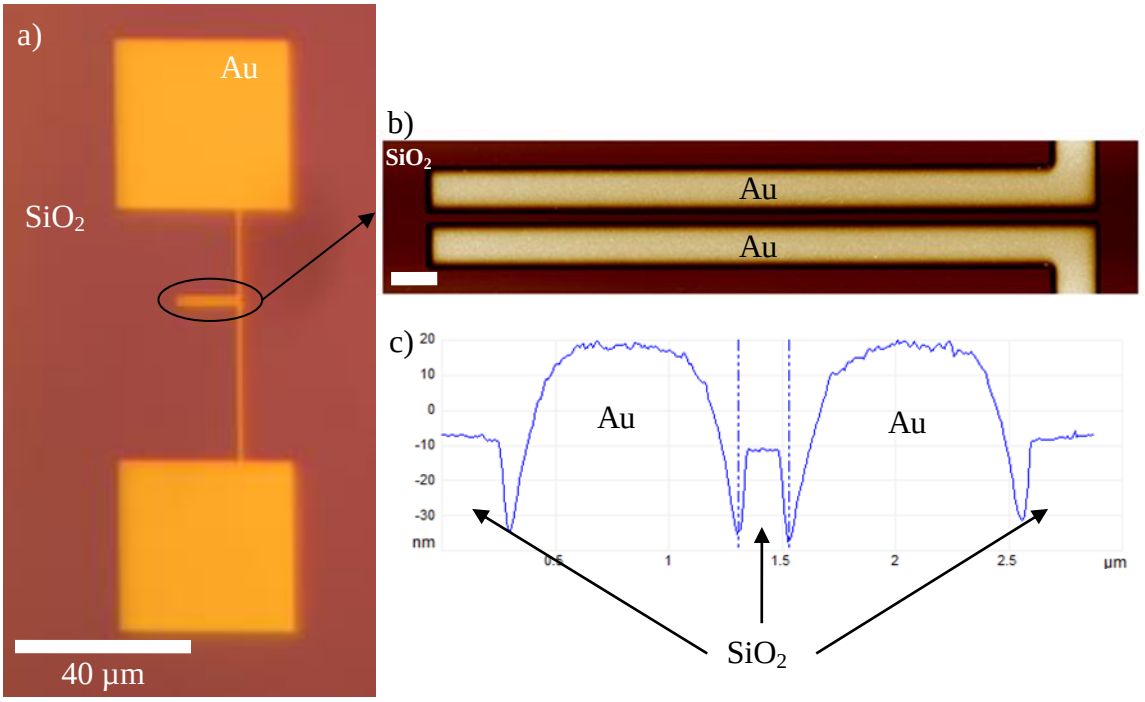

Figure 3.4 (a) Optical micrograph of the parallel Au electrode structure. (b) AFM height image of the Au finger electrodes of the parallel electrode section. Scale bar = 1 µm (c) Cross sectional height of the Au finger electrodes obtained from AFM height data. The gap between the Au electrodes is ~250 nm and the Au electrodes are ~50 nm tall.

3.4 Bare Nanotubes Deposition, Au enhancement, and DC-IV Measurement

Placement of the DNA NTs across the parallel Au electrode fingers is essential to performing electrical characterization and determining the extent of electrical conductivity. Direct deposition, via pipetting, of DNA nanotubes on the Au electrodes was the primary technique used to facilitate the bridging of DNA nanotubes. It is expected that the bare DNA NTs will not be conductive and act as an insulator, thus the NTs would create a suitable substrate for the attachment of AuNPs that act as the only conduction path for the current to flow.

The conductivity of bare DNA origami NTs was measured and compared under the following two scenarios: (1) a Au electrode structure prior to any deposition of NTs and (2) the DNA origami NTs following Au enhancement. A DC-IV measurement of a bare Au electrode structure is shown in Figure 3.5c as the solid black curve. The current at any bias is below 1 fA, which is the detection limit of the Keithley 4200 SCS. Hence, the electrode structure is non-conductive as expected. Subsequently, a solution of 5 nM bare DNA origami NTs was deposited onto the electrode structure. Figure 3.5a shows an AFM height image of bare DNA origami NTs bridging the electrodes and Figure 3.5b is a magnified AFM height image of the area highlighted in the green circle. There are 3 bare NTs observed bridging the electrodes. Current-voltage measurements were performed on the bare NTs as shown by the dotted red curve in Figure 3.5d. Following electrical measurements of the bare NTs, the same NTs were immersed in Au enhancement solution for 10 minutes using the methods described in Chapter 2.2.2 to ensure the bare NTs cannot be Au enhanced. If the bare NTs can be Au functionalized from the enhancement solution, unwanted shorting of the electrodes could occur and affect DC-IV

measurements of the Au functionalized DNA NTs. Figure 3.5c shows a magnified AFM height image of same area highlighted in green in Figure 3.5a of the bare DNA origami NTs following a 10 minute immersion in Au enhancement solution. The AFM image does not reveal evidence of Au enhancement of the DNA NTs. Electrical measurements of the bare NTs exposed to Au enhancement solution were electrically characterized as shown by the green curve in Figure 3.5d. The measured current of the bare NTs before and after exposure to the Au enhancement solution are in the femtoamps range. The corresponding resistance is in the 10^{12} Ω range. The IV data, as does the AFM data, provides compelling evidence that the Au enhancement solution does not result in Au deposition on the bare DNA NTs. These results are consistent with the expected outcome. The bare NTs are a suitable substrate for the attachment of AuNPs because the bare NTs are not electrically conductive. Also, the NTs cannot act as a substrate on which the Au enhancement solution can attach and result in undesired bridging of the electrode structures, showing the Au enhancement solution only enhances Au.

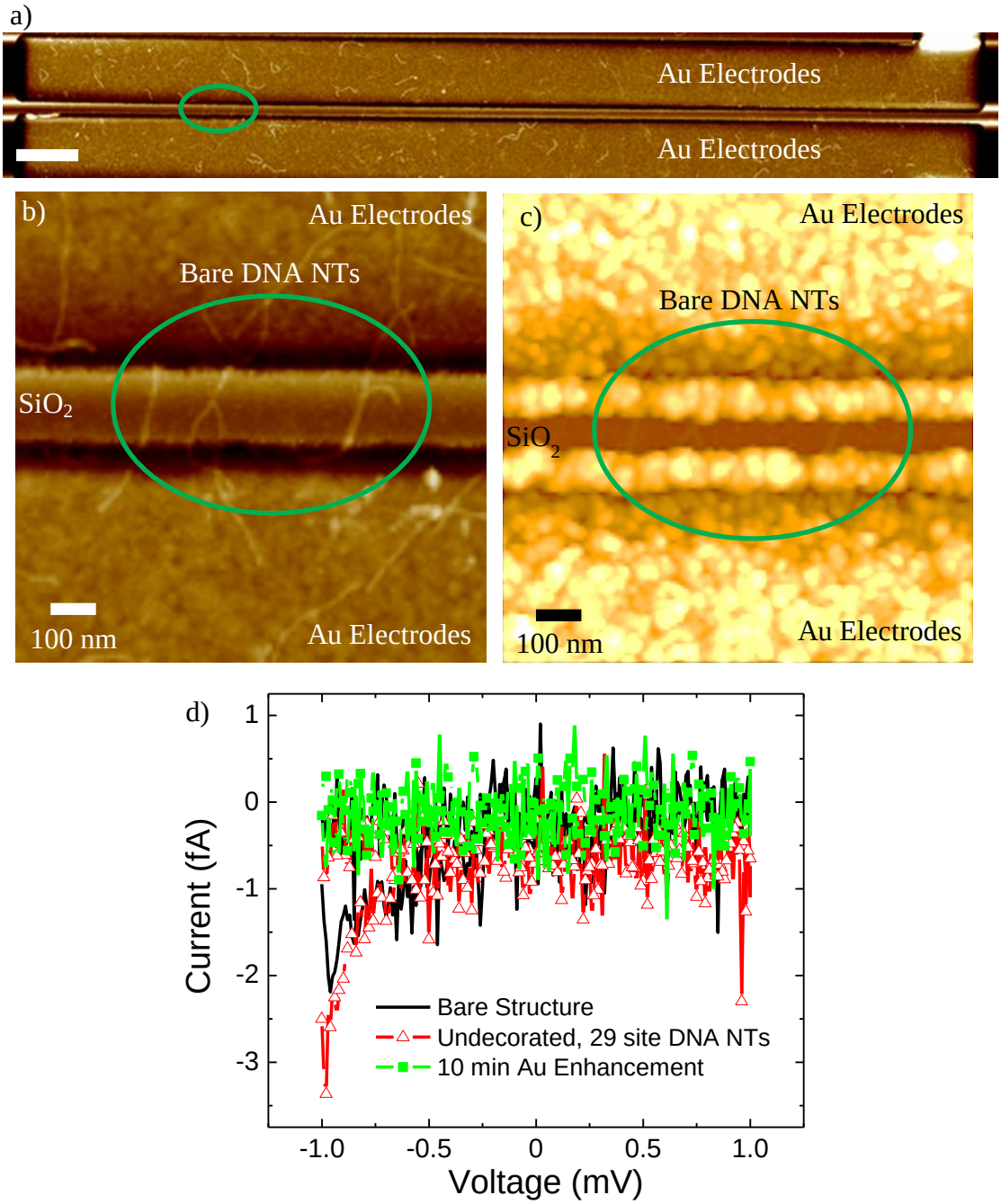

Figure 3.5 (a) AFM height image of an electrode structure with several bare, DNA origami NTs bridging the electrodes. Scale bar = 1 µm (b) Magnified AFM height image of the bridging bare NTs highlighted in the green circle from Figure 3.5a. (c) Magnified AFM height image of the same NTs highlighted in the green circles from Figure 3.5a and b that was Au enhanced for 10 minutes. There is no observed shorting of the electrodes from the Au enhancement solution and the bare NTs (d) DC-IV measurements of the electrode structure with bare NTs deposited, and after 10 minutes of Au enhancement. The hysteresis is due to the trap charges not having enough time to detrap.

3.5 AuNP DNA Origami Nanotube Deposition, Au enhancement, and DC-IV Measurement

To examine the conductivity of a single AuNP functionalized DNA origami NT, NTs decorated with 5 nm diameter AuNPs were deposited onto the electrode structures by direct deposition via pipetting. AFM was subsequently performed to reveal successful bridging NTs and expose any debris that might compromise the electrical measurements. Successful bridging of a single NT was observed on at least 5 different electrodes. An example of a successful bridging structure is highlighted in the white circle in Figure 3.6a. Additional NTs and AuNPs were observed within the gap between the electrodes as highlighted in the black, dashed circle in Figure 3.6a. Nanomanipulation using Bruker's NanoMan, a technique of moving, manipulating, and scratching nanoscale-sized objects, was used to remove unwanted NTs and debris from the gap between the Au electrodes [73]. Several DNA NTs were removed from the gap as demonstrated in the electrode gap area highlighted in the black, dashed circle in Figure 3.6b. With the excess NTs and debris removed from the gap, the only possible conduction is through the remaining AuNP decorated DNA NT.

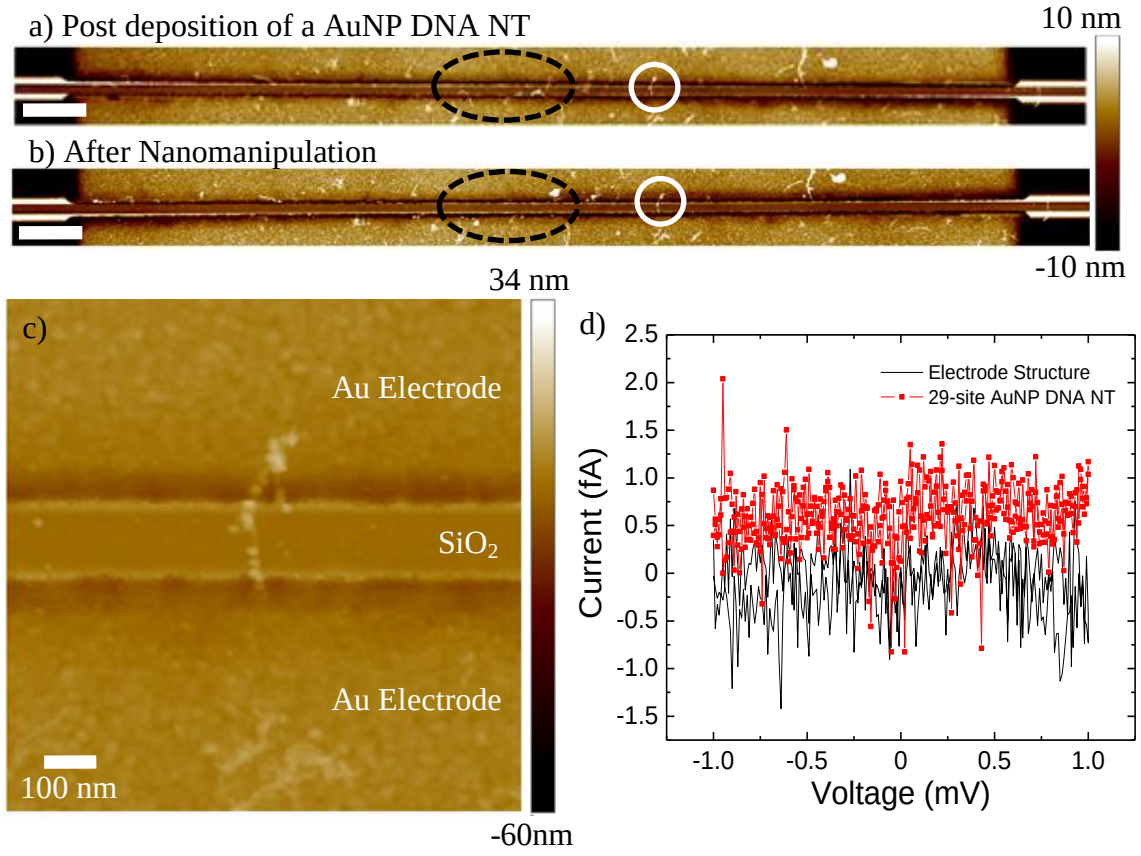

Figure 3.6 (a) Parallel finger electrodes bridged by a single, decorated DNA NT (white circle). The black dashed circle highlights unwanted NTs and debris after deposition. Scale bar = 1 µm (b) Parallel finger electrodes following removal of debris and unwanted NTs using AFM nanomanipulation (black dashed circle), leaving only the single NT bridging the gap (white circle). Scale bar = 1 µm (c) Magnified AFM height image of the NT bridging the Au finger electrodes shown in Figure 3.6a and b in the white circle. There are approximately 7-8 AuNPs spanning the gap. (d) An example of a DC-IV measurement of a bare parallel electrode structure and a decorated DNA origami NT. The AuNP DNA NT is not conductive.

Figure 3.6c is a magnified AFM height image of the AuNP DNA NT bridging the electrodes. There are approximately 7 to 8 AuNPs spanning the gap between the electrodes, 5-6 AuNPs spanning the SiO_2 gap, and 2 AuNPs within the valleys between the Au electrodes and the SiO_2. With an expected AuNP attachment yield of ~55-58%

and a measured gap size of ~220 nm of the device shown in Figure 3.6c, ~8 AuNPs were expected to be spanning the gap.

DC-IV measurements showed the AuNP DNA origami NTs were not electrically conductive and Figure 3.6d is a representative DC-IV measurement. The measured electrical current of the AuNP DNA NT was similar to the measurement of the bare electrode structure as both were in the fA range and had resistances in the $10^{12}\,\Omega$ range. Note that these low currents are similar to the bare NTs shown in Figure 3.5c.

To enhance the electrical response of the deposited NTs, the single AuNP DNA NT bridging the parallel Au finger electrodes was enhanced using a solution containing Au ions as described in Section 2.2.4 Au Enhancement of AuNPs and Au Clusters. Au enhancement increases the size of the AuNPs and therefore reduces the spacing between AuNPs. Displayed in Figure 3.7a is an AFM height image of a decorated DNA NT bridging the electrode structure that has been Au enhanced for 15 minutes. The electrodes were also Au enhanced because the Au enhancement solution is deposited directly on the electrode structure. Figure 3.7b is a magnified AFM height image of the Au enhanced AuNP DNA NT highlighted in the white circle in Figure 3.7a while Figure 3.7c is an SEM image of the same NT shown in Figure 3.7a and b. The average height of the Au enhanced AuNPs of the NT shown in Figure 3.7a-c is ~82.7 nm and the width perpendicular to the NT, referred to as perpendicular width, is ~117.8 nm. The average height was determined from Figure 3.7b and the perpendicular width was determined from Figure 3.7c. Following the Au enhancement, the gap between the electrodes in Figure 3.7c decreased by 152 nm to ~68 nm from a gap of ~220 nm prior to the Au enhancement. After Au enhancement, the NT is no longer visible and only the AuNPs are

visible and appear to have merged together. The AuNP growth due to Au enhancement is non-uniform but the NT is a continuous structure that is electrically conductive.

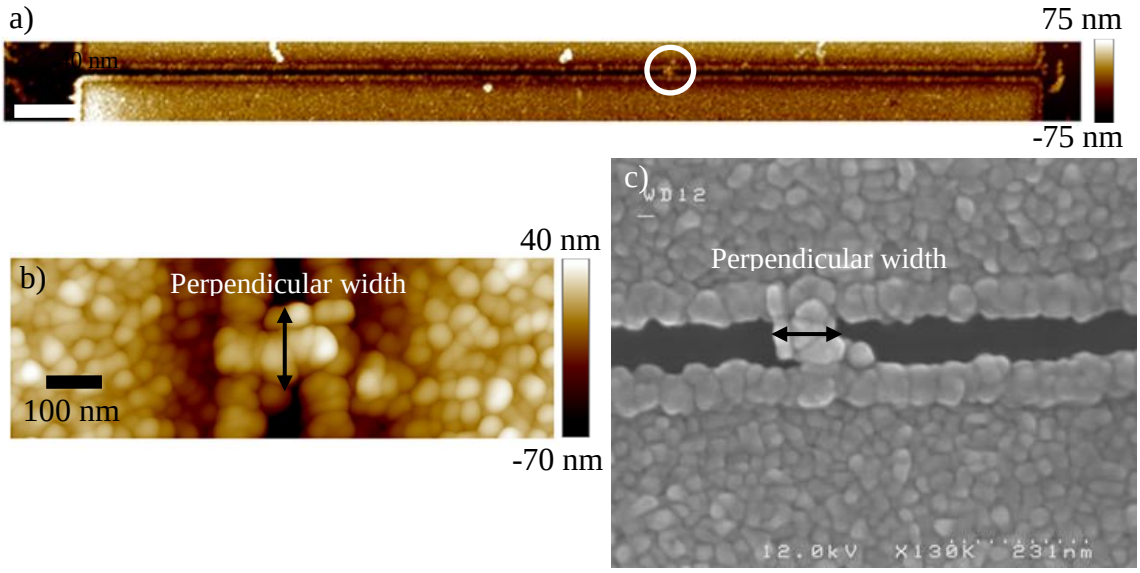

Figure 3.7 (a) AFM height image of the 15 min Au enhanced parallel electrode structure with a AuNP DNA NT bridging the electrodes shown in Figure 3.6a and b. (b) AFM height image of the 15 min. Au enhanced NT shown in Figure 3.7a. The black arrow shows what is defined as the perpendicular width. (c) SEM image of Au enhanced NT in Figure 3.7a.

After a 15 minute exposure to the Au enhancement solution, the AuNP DNA NTs were electrically tested and exhibited linear, ohmic behavior with resistances ranging from 60 Ω to 8 MΩ for five different devices. The results are listed in Table 3.2. The device shown in Figure 3.6 and Figure 3.7 is listed as device 4 in the table. Figure 3.8a shows the results of the DC-IV curves for the two NTs with resistances in the MΩ range while Figure 3.8b shows the DC-IV curves for the three NTs that had resistances of ~60 Ω. After the devices were SEM imaged, the resistance of devices 1 and 2 decreased from MΩ to 170 Ω and 80 Ω, respectively, as shown in Figure 3.9. Device 4 also experienced a small decrease in resistivity from 64 Ω to 48 Ω.

Table 3.2 Measured resistances and dimensions for AuNP Decorated DNA NT devices after 15 minute of Au Enhancement.

Device	# of AuNP Spanning the gap	Initial Measured Resistance	Measured Resistance Post-SEM Imaging	Average Au Enhanced AuNP Decorated DNA NT Height^{+} (Δ change)	Average Au Enhanced AuNP Decorated DNA NT Width* (Δ change)	Au Enhanced NT Bridging Length^
1	4	~ 8 MΩ	~ 170 Ω	51.2 nm (18.9 nm)	38.3 nm (18.5 nm)	132.8 nm
2	5	~ 1 MΩ	~ 82 Ω	61.6nm (37.4 nm)	65.9 nm (49.3 nm)	131.9 nm
3	6-7	~ 64 Ω	~ 60 Ω	67.4 nm (21.7 nm)	109 nm (60 nm)	129 nm
4	7-8	~ 64 Ω	~ 48 Ω	82.7 nm (22.2 nm)	117.8 nm (112.1 nm)	118.9 nm
5	5-6	~ 60 Ω	~ 60 Ω	79 nm (22.1 nm)	80 nm (37.5 nm)	190 nm

+: Measurements obtained from AFM height data

*: Measurements obtained from SEM images. Unconstrained/perpendicular width (i.e., perpendicular to nanotubes) was measured.

^: Measurements obtained from SEM images of Au enhanced NT bridging the parallel electrode structure.

a)

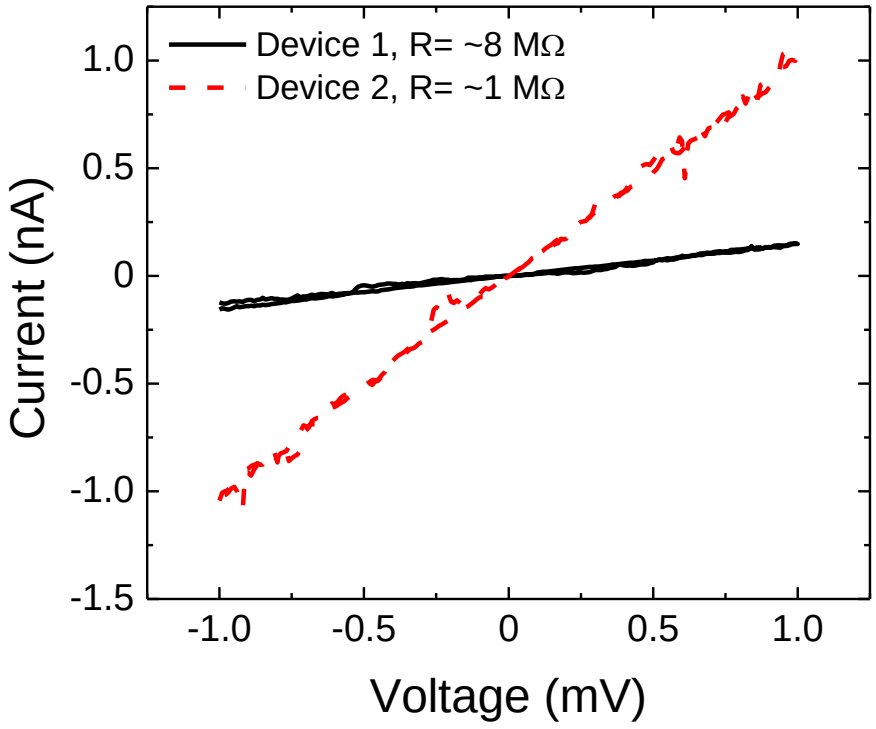

b)

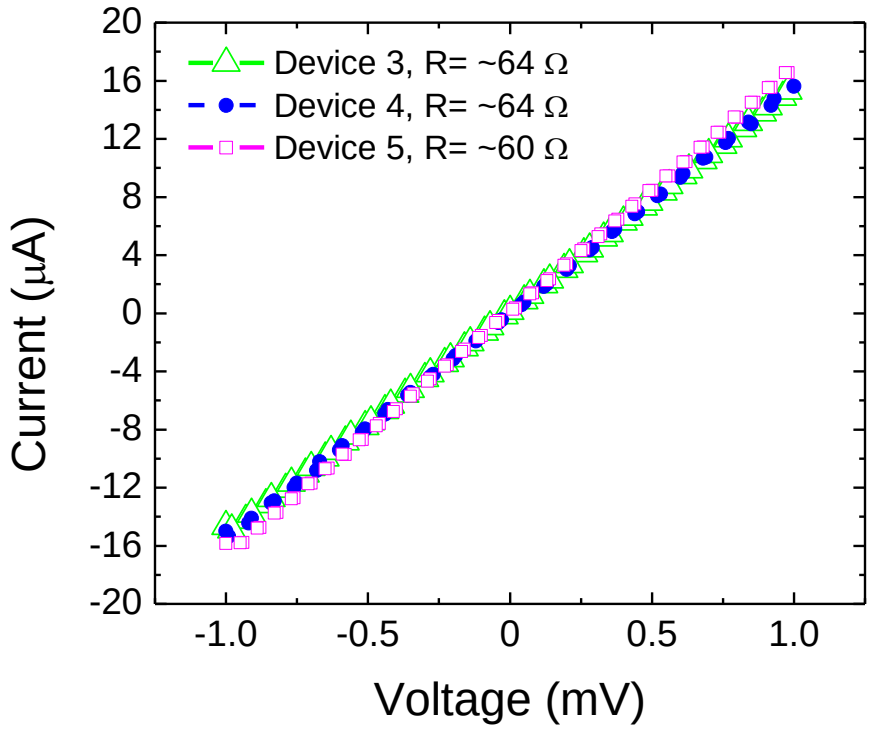

Figure 3.8 DC-IV measurement from -1 mV to 1 mV and back to -1 mV for single AuNP DNA NTs Au enhanced for 15 minutes. (a) Devices 1 and 2 have resistances in the MΩ range. (b) Devices 3-5 have resistances in the 60 Ω range.

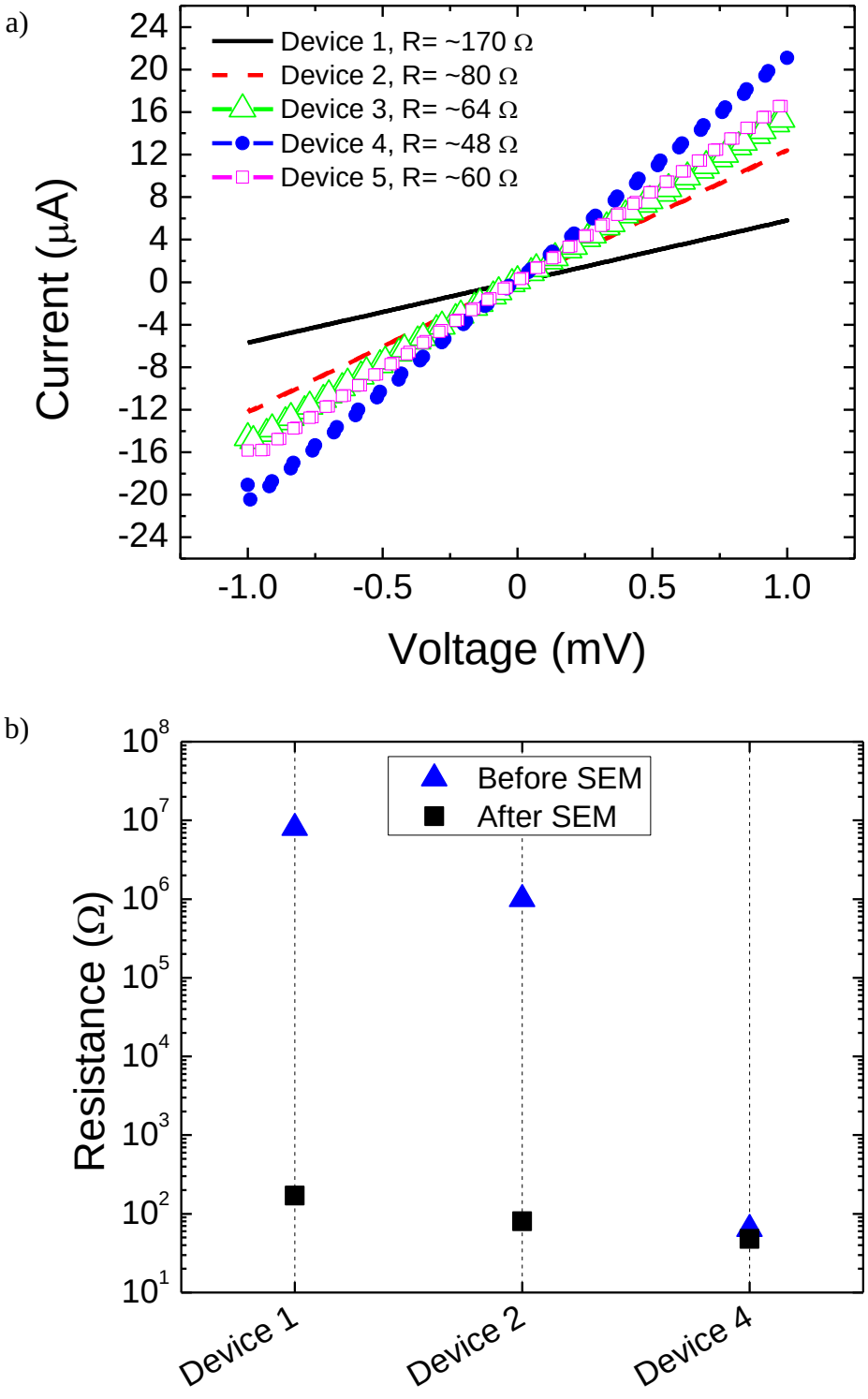

Figure 3.9 (a) DC-IV measurements from -1 mV to 1 mV and back to -1 mV for single AuNP DNA NTs enhanced for 15 minutes after the devices were SEM imaged. The resistances range from 48 Ω to 170 Ω. (b) Comparison of the measured resistance of the devices 1, 2, and 4 before and after SEM imaging.

To determine if the electrical conduction observed in the devices was only possible through the Au enhanced AuNP DNA NT and not by other means (e.g., closed gap, free NPs, etc.), the Au enhanced AuNP DNA NT connecting device 3 was removed using AFM nanomanipulation (APPENDIX B.2). Figure 3.10a and b are AFM height images of the Au enhanced NT before and after being removed using AFM nanomanipulation, respectively. The DC-IV measurements shown in Figure 3.10c demonstrate that the electrode structure is no longer conductive as the current has returned to the fA range and the resistance is in the 10^{12} Ω range. The evidence clearly confirms that the Au enhanced DNA NT was the only conduction path for the current to flow.

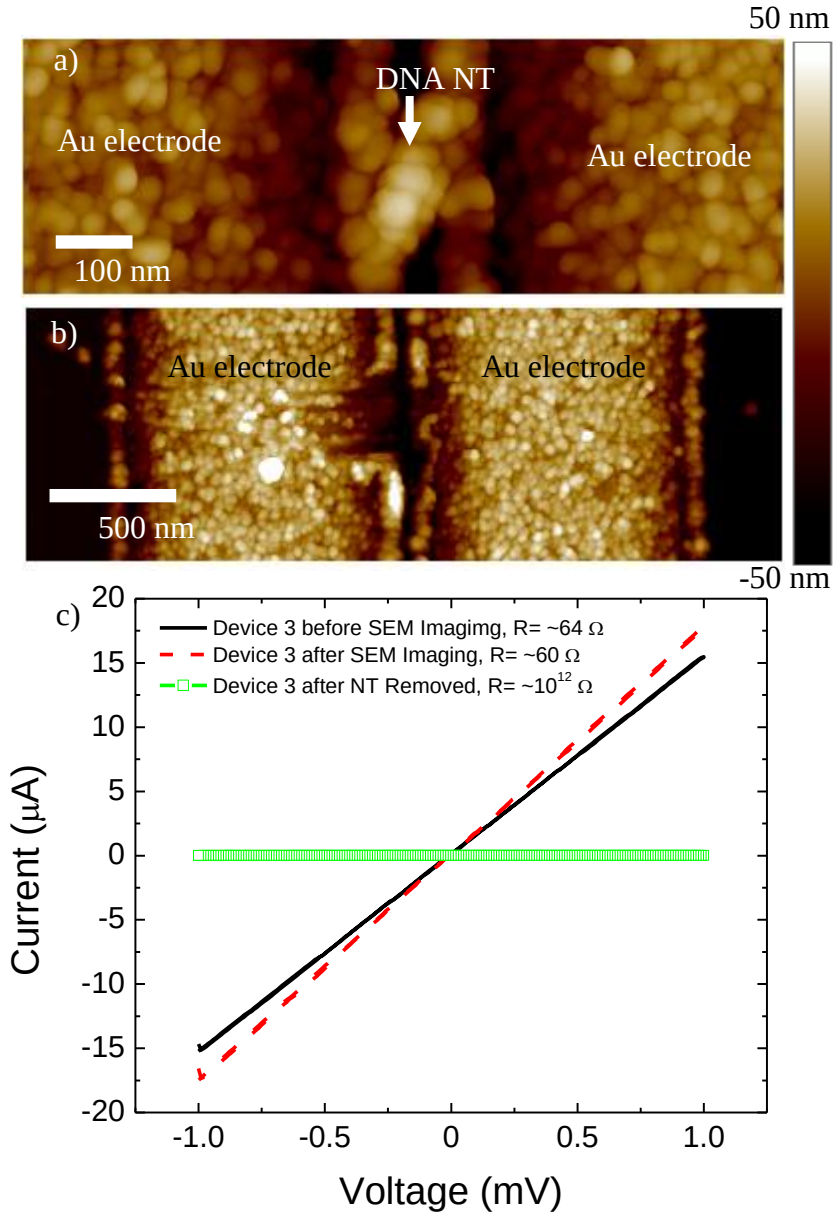

Figure 3.10 (a) AFM height image of the 15 minute, Au enhance AuNP DNA NT bridging the electrodes of device 3. (b) AFM height image of the NT shown in Figure 3.10a after being removed using nanomanipulation. (c) DC I-V response of before and after the removal of the bridged Au enhanced DNA NT for Device 3. With the Au enhanced NT removed, the electrode structure is highly resistive, demonstrating conduction was through the NT.

3.6 Au Seeded DNA Origami Nanotube Deposition, Au Enhancement, and DC-IV Measurement

Positively charged Au clusters were used as an alternative method to AuNPs to functionalize the DNA origami NTs towards creating conductive nanowires. Au seeded NTs were deposited onto the parallel electrode structure and nanomanipulation was used to remove any debris and unwanted NTs. The metallized NTs were observed bridging the parallel Au finger electrodes. Figure 3.11a shows 2 Au seeded NTs bridging the electrodes after direct deposition via pipetting, which will be referred to as S2. From the AFM images shown in Figure 3.2a and Figure 3.11a, it appears that the Au seeding resulted in small seeds or grains of Au approximately 9 nm in height. The results of DC-IV measurements of the Au seeded NTs shown in Figure 3.12 indicates that the NTs were not conductive as evidenced by the currents in the single femtoamps and resistances of 10^{12} Ω. Note that the low currents and the high resistances observed here are similar to the decorated NTs prior to Au enhancement. From AFM height images shown in Figure 3.2a, the Au seeds appear to be covering the surface of the NTs, but evidently the coverage is not sufficient enough to create a conductive NT.

S2 shown was subsequently subjected to Au enhancement for 5 minutes to increase the size of the Au seeds and possibly promote electrical conduction. Figure 3.11b is an AFM height image of S2 after 5 minute Au enhancement. The Au enhancement was performed directly on the electrode structure with the bridging NTs. As a result, the Au deposited on the electrodes was also Au enhanced. Figure 3.11e is a magnified AFM height image of the NT labeled #2 in Figure 3.11b following 5 minutes of Au enhancement. The Au enhanced Au seeds have the similar non-uniform surface

morphology as observed with the Au enhancement of AuNP DNA NTs. The measured maximum cross section height of the 5 minute Au enhanced Au seeded NT at the white dotted line shown in Figure 3.11e is ~21 nm, but the Au enhanced Au seeds do not appear to have merged with each other as shown in the cross section of the blue dotted line of Figure 3.11e. The result of the DC-IV measurement of the 5 minute Au enhanced device S2 shown in Figure 3.12 demonstrate that the enhanced NTs remain nonconductive and have a similar resistance of ~10^{12} Ω to the Au seeded NTs before Au enhancement. The very high resistance is most likely due to the apparent separation of the Au seeds observed in Figure 3.11e.

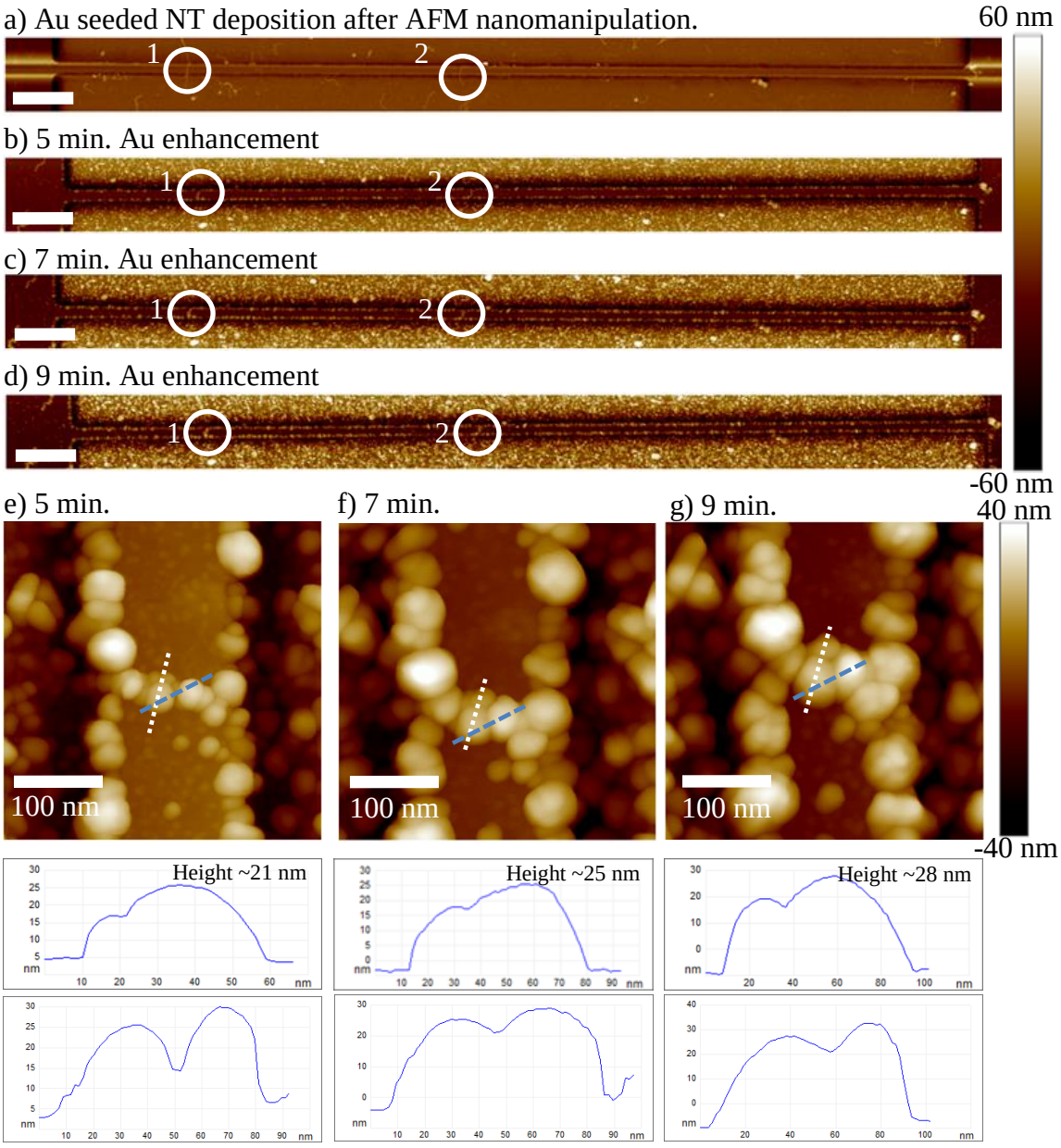

Figure 3.11 AFM height image of deposited, Au seeded NTs. The device is referred to as S2. (a) After performing nanomanipulation to clear debris and unwanted NTs with two NTs bridging the electrodes. (b) After 5 min. Au enhanced Au seeded NTs. (c) After 7 min. total Au enhanced Au seeded NTs. (d) After 9 min. total Au enhanced Au seeded NTs. Scale bar for a-d = 1 µm (e) AFM height image of the 5 min. Au enhanced Au seeded NT labeled 2 in Figure 3.11a-d and cross sectional height at tallest point (white dashed line) and across the seeds (blue dashed line). (f) AFM height image of the 7 min. Au enhanced Au seeded NT labeled 2 in Figure 3.11a-d and cross sectional height at the tallest point and across the seeds. (g) AFM height image of the 9 min. Au enhanced Au seeded NT labeled 2 in Figure 3.11a-d and cross sectional height at the tallest point and across the seeds.

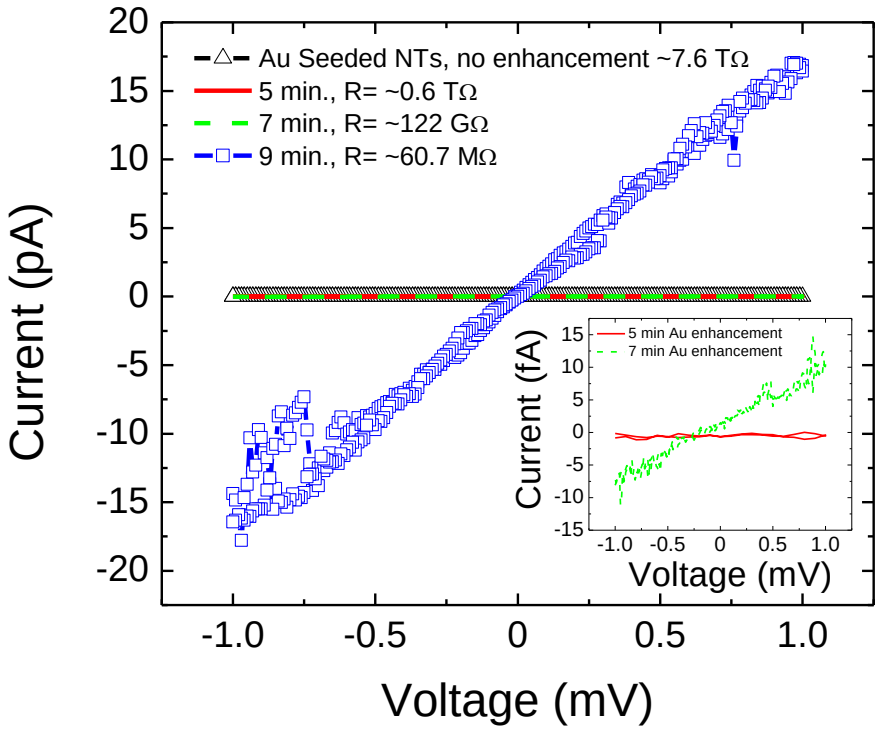

Figure 3.12 DC-IV of the NTs shown in Figure 3.11. Inset is the 7 min. total Au enhancement of the Au seeded NTs. Resistance of the device decreased after each Au enhancement, indicating it may be possible to control the conductivity of the Au seeded NT by adjusting the size of the AuNPs.

Two additional Au enhancements were performed on S2 to increase electrical conductivity. Each Au enhancement was performed for a period of 2 minutes, for a total Au enhancement time of 7 and 9 minutes, respectively. For each of the Au enhancement times, AFM height images reveal an increase in Au seed size of the NTs as shown in Figure 3.11c and d. Figure 3.11f is a magnified AFM height image of the Au seeded NT labeled #2 from Figure 3.11c after 7 minutes of Au enhancement. The height of the Au seeds in the same measured cross section as Figure 3.11d has increased from 21 nm to 25 nm and the Au seeds appear to have merged together creating possibly a conductive device. The DC-IV measurement of S2 Au enhanced for a total of 7 minutes confirms it

was electrically conductive showing a resistance of ~122 GΩ. The inset graph of Figure 3.12 shows the DC-IV curve of the 7 minute Au enhancement of the Au seeded NT along with the 5 minute data as a reference. The DC-IV data of the 7 minute Au enhancement exhibited a linear, ohmic response; however, the current was in the low fA.

Figure 3.11g is a magnified AFM height image of the Au seeded NT labeled #2 from Figure 3.11d after 9 minutes of Au enhancement. Though the height of the enhanced Au seeds only increased from 25 nm to ~28 nm, the perpendicular width of the Au seed's cross section has grown from ~68 nm to ~97 nm (AFM lateral resolution > 5 nm). The Au seeded NT's electrical resistance decreased from ~122 GΩ to ~60.7 MΩ after 9 total minutes of Au enhancement as shown in Figure 3.12. By performing additional Au enhancements, it may be possible to control the conductivity of the Au seeded NTs and further reduce the resistance by increasing the size of the Au seeds with Au enhancements.

A second device, S3, with 3 bridging seeded NTs was also Au enhanced and electrically characterized using DC-IV measurements. It was enhanced for 5, 7, and 9 total minutes. Figure 3.13 shows the AFM and SEM images of S3 Au enhanced for 9 minutes.

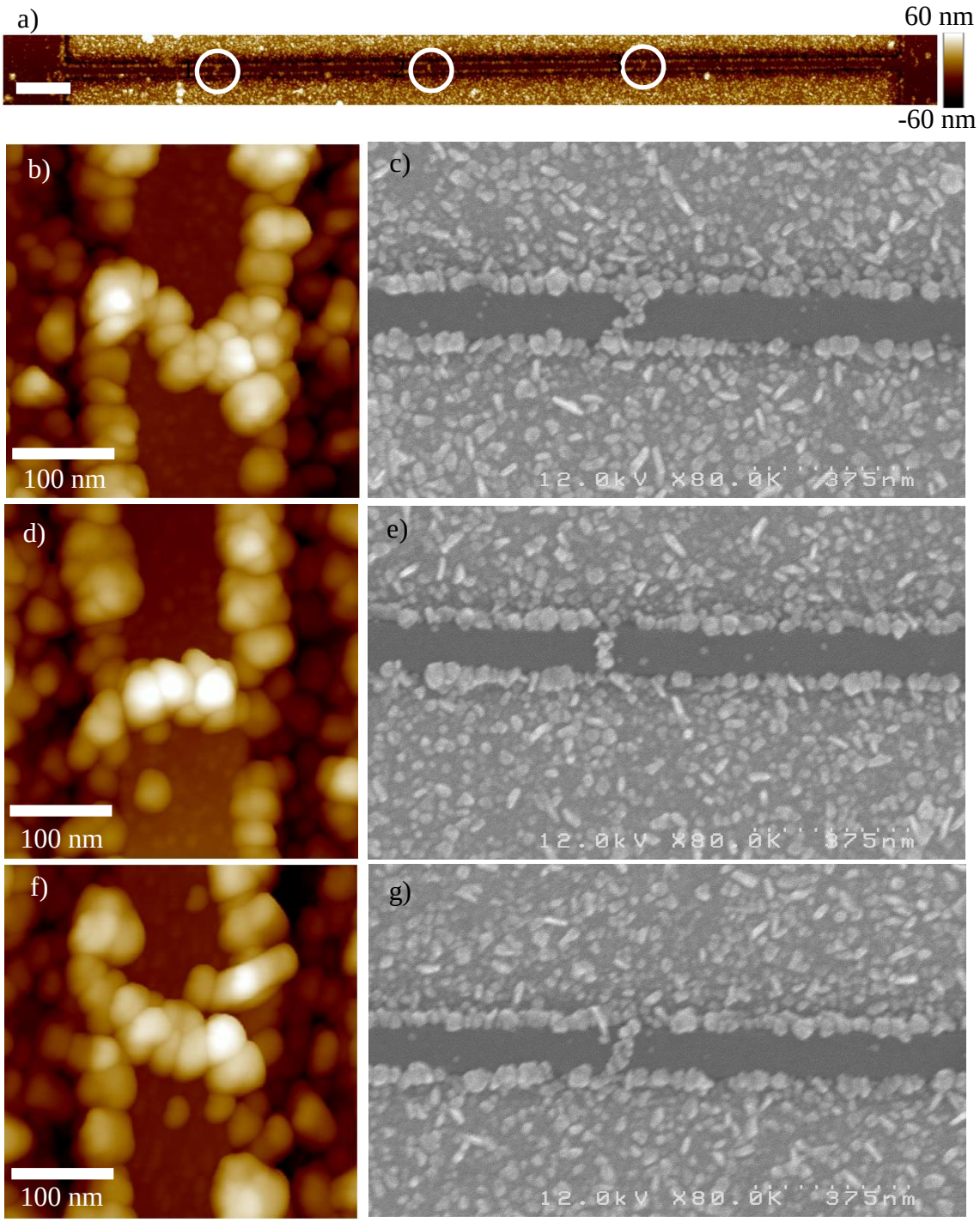

Figure 3.13 (a) AFM height image of S3 enhanced for 9 minutes. Scale bare = 1 µm (b) AFM height image of NT labeled 1 in Figure 3.13a and (c) corresponding SEM image. (d) AFM height of NT labeled 2 in Figure 3.13a and (e) corresponding SEM image. (f) AFM height of NT labeled 3 in Figure 3.13a and (g) corresponding SEM image. The growth of the Au seeds is similar to the growth of the AuNPs because both show non-uniform growth

The DC-IV data of S3 after a total of 7 and 9 minutes of Au enhancement is shown in Figure 3.14. The inset of Figure 3.14 is the DC-IV data of S3 after 7 minutes of Au enhancement. An increase in electrical conduction was observed following each Au enhancement similar to the S2.

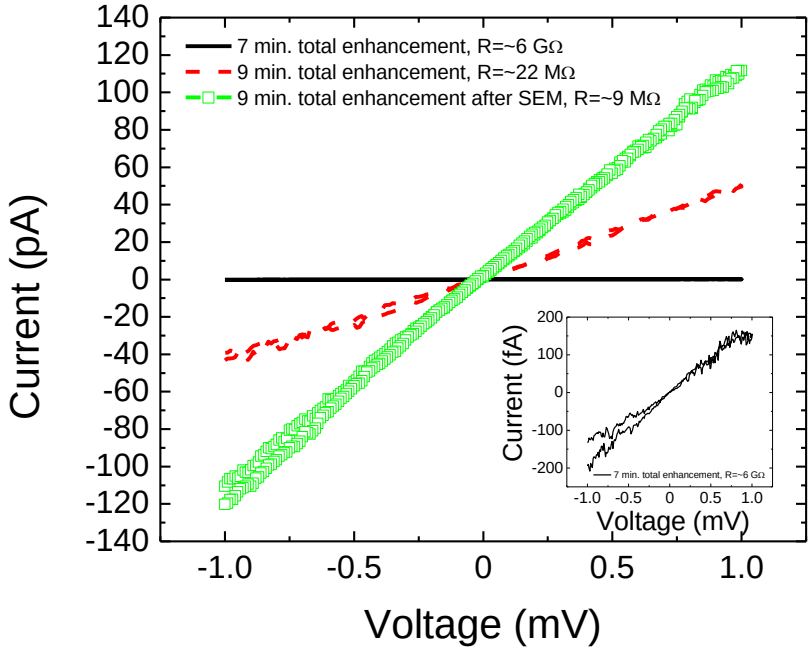

Figure 3.14 DC-IV of an electrode structure bridged by 3 Au seeded NTs. Inset is the 7 min. total Au enhancement. Resistance of the device is reduced after each Au enhancement. Au seeded NTs and 5 min. Au enhancement were not conductive with resistances over TΩ (not shown to provide clarity).

S3 prior to Au enhancement and after 5 minutes of Au enhancement was not conductive with resistances in the TΩ, which was similar to S2. After 7 minutes of Au enhancement, conduction was observed and S3 exhibited a resistance of ~6 GΩ. The resistance decreased further to ~22 MΩ after 9 minutes of Au enhancement. The measured

resistances of S3 were less than the measured resistances of S2 after 7 and 9 minutes of Au enhancement (~122 GΩ and ~60.7 MΩ).

Table 3.3 provides a compilation of all the measured resistances of the Au seeded DNA NTs and the height and width measurements from AFM data.

Table 3.3 Measured Resistance and Dimensions (from AFM scans) of Au seeded DNA NTs for Different Au Enhancement Times (Before SEM Imaging)

Device	Total Au Enhancement Time	Measured Resistance	Average AFM Height of all NTs (Δ Change)	Average AFM Width of all NTs (Δ Change)*
S2	0 minutes	TΩ	N/A	N/A
S2	5 minutes	TΩ	23.8 nm (19 nm)	46 nm (15 nm)
S2	7 minutes	~122 GΩ	32.1 nm (29 nm)	68.7 nm (35.4 nm)
S2	9 minutes	~60.7 MΩ	42.9 nm (34.5 nm)	78.2 nm (43.4 nm)
S3	0 minutes	TΩ	N/A	N/A
S3	5 minutes	TΩ	21.7 nm (14.5nm)	46 nm (28.3 nm)
S3	7 minutes	~6 GΩ	31.5 nm (16.1 nm)	65.2 nm (25.3 nm)
S3	9 minutes	~22 MΩ	39.3 nm (18.1 nm)	73.8 nm (21.7 nm)

*: Unconstrained/perpendicular width (i.e., perpendicular to nanotubes) was measured.

S3 was also imaged using SEM after being Au enhanced for 9 total minutes. Figure 3.13c, e, and g are SEM images of S3 after 9 total minutes of Au enhancement. Table 3.4 presents the dimensions of each NT after 9 minutes of Au enhancement. The devices were electrically characterized after SEM imaging to determine if the resistance also decreased as the resistance had with the AuNP DNA NTs. The resistance decreased from ~22 MΩ to ~9 MΩ. S2 was not SEM imaged because it was damaged after DC-IV testing and was not useable.

Table 3.4 Dimensions of the 9 total minute Au enhanced Au seeded DNA NTs (Figure 3.13)

Au seeded DNA NT	Average Height[+]	Average Width*	Length[^]
1	32.4 nm	46.3 nm	108.4 nm
2	44.8 nm	41.2 nm	115.2 nm
3	36.1 nm	42.9 nm	122 nm

+: Measurements obtained from AFM height data

*: Measurements obtained from SEM images. Unconstrained/perpendicular width (i.e., perpendicular to nanotubes) was measured.

^: Measurements obtained from SEM images of Au enhanced NT bridging the parallel electrode structure.

CHAPTER FOUR: DISCUSSION

The objective of this thesis is to determine the viability of fabricating an electrically conductive Au functionalized DNA origami NTs by adjusting the size of the (1) AuNPs or (2) Au seeds on a DNA origami NT. To test this hypothesis, DNA origami NTs with 29 binding sites for AuNPs were synthesized and functionalized with 5 nm diameter AuNPs. Positively charged 1.4 nm diameter Au clusters in solution were also used as alternative method of metallizing (i.e., seeding) the NTs instead of AuNPs. Au enhancement solution was used to enlarge the AuNP functionalized NTs and Au seeded NTs. Electrode structures were fabricated to interface the DNA NTs with electrical characterization instrumentation. The NTs were deposited onto the electrode structures using direct deposition via pipetting. Process evaluation and verification was performed using AFM, SEM, TEM, and DC-IV electrical characterization.

A summary of the findings is briefly provided before discussing the results in detail. DC-IV electrical measurements showed that the bare DNA origami NTs were not conductive, indicating the bare NTs could be used as a suitable non-conducting substrate for attaching AuNPs. As-synthesized AuNP DNA NTs with 18-20 AuNPs attached were electrically characterized and found to be non-conductive. Subsequent Au enhancement, an electroless Au deposition process, was used to enhance the electrical response of the DNA origami NTs by increasing the size of the AuNPs. After 15 minutes of Au enhancement, the Au enhanced AuNP DNA NTs exhibited resistances between 60 Ω to 8

MΩ. Subsequent to SEM imaging of the Au enhanced AuNP DNA NTs, it was observed that the resistances of four out of the five NTs decreased to between 48 Ω to 170 Ω.

DNA origami NTs seeded with the positively charged Au clusters were also deposited onto the parallel electrodes and electrically characterized. Two electrode structures were observed with successful DNA origami NTs bridging of the electrodes: one device with 2 bridging NTs, and the other device with 3 bridging NTs. Both devices exhibited very little conductivity before Au enhancement. Au enhancement was used to increase the electrical response. Au enhancement times of 5, 7, and 9 minutes were performed. Conductivity was only observed after a total of 7 minutes of Au enhancement with a resistance in the GΩ range for each device. Following 9 minutes Au enhancement, the resistance decreased to the MΩ range for each device. The device with 3 NTs bridging the electrodes also saw a decrease in resistance after imaging using SEM.

4.1 Optimal Electrode Structure Design to Achieve DNA Origami Nanotube Bridging

Optimizing the design of the electrode structures and the method to deposit the NTs across the electrodes was critical because access to the NTs was required for electrical DC-IV characterization. The design criteria for the electrode structures included (1) maximizing the probability of DNA origami NTs bridging and (2) increasing the probe pad size and increasing the probe pad resistance to damage during probing. The Au electrode structure design evolved via several iterations to assess the best electrode structure for increasing the probability of NT bridging during the course of this thesis.

Figure 4.1a is a schematic of the original electrode structure with dimensions and an AFM amplitude image of the pointed electrodes and exposed window. The electrode structure was coated with PMMA to lithographically expose a window over the gap area to force the DNA origami NTs to bridge only over the gap between the electrode tips. The probability of bridging a AuNP decorated DNA NT in the window across the pointed electrode gap of the first electrode structure was small due to the low concentration of the AuNP DNA NTs and was further inhibited by the small area of the gap between the electrode tips. The concentration of the DNA NTs was low because of the multiple filtration steps required to remove excess DNA staple strands and AuNPs from the DNA NT solution. The final concentration of the filtered AuNP decorated DNA NT solutions was less than 1 nM and was determined to be too low to expect appreciable probability of successful DNA origami NT bridging across the pointed electrode structures.

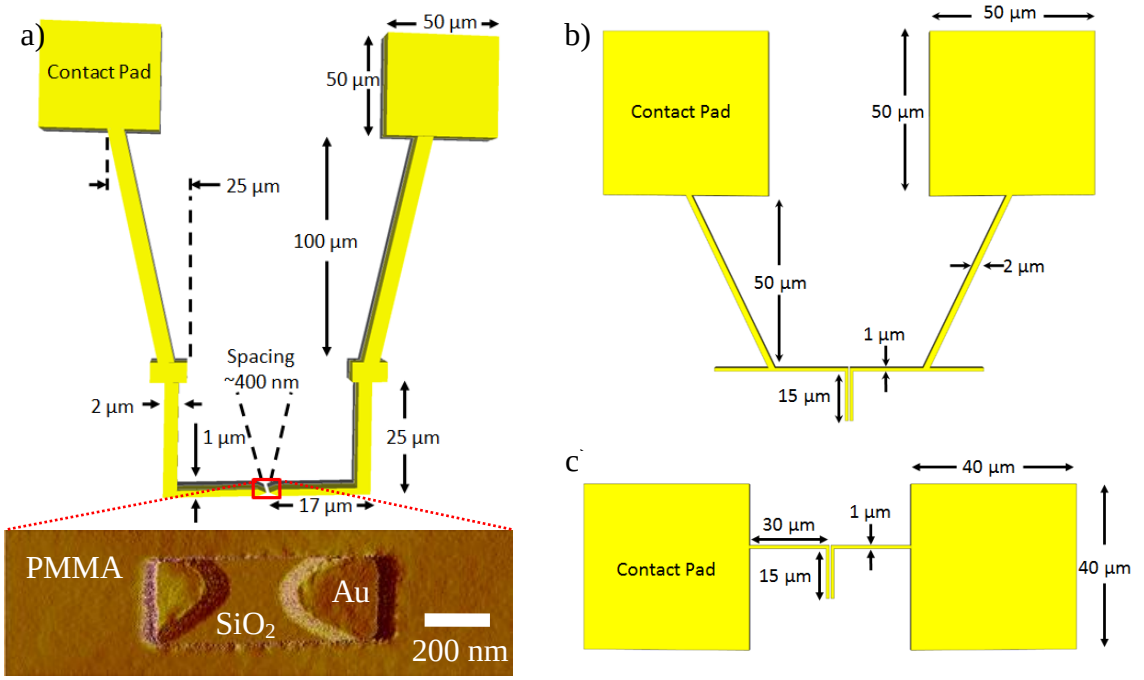

Figure 4.1 (a) Schematic of the electrode structure with pointed electrodes and a 350-400 nm gap. The gap between the electrodes was exposed in the PMMA. The inset is an AFM amplitude image of the electrode gap; (b) Schematic of the parallel electrode structure with the longer electrodes connecting the contact pads and the parallel finger electrodes; (c) Schematic of the final Au electrode structure without the electrode legs and smaller contact pads (40 µm x 40 µm).

To experimentally establish the lowest possible NT concentration that bridging could occur on the first electrode structure, a range of concentrations of bare DNA origami NTs were deposited onto the structures. The probability targeted for bridging was selected as one out of five times because of mitigating factors that included (1) the significant amount of time required to fabricate the electrode structures, (2) the low availability of the electrode structures, and (3) the low availability of Au functionalized DNA NTs because the amount of Au available was low at times. The bare NTs were deposited in the same manner as described in Section 2.2.6 DNA Origami Nanotube Deposition. It was observed that, at NT concentrations of ≤1 nM, the NTs were not

bridging the pointed electrodes. For example, as shown in Figure 4.2a, bridging of DNA origami NTs was not observed following deposition of a ~0.83 nM solution on the pointed electrode structure. Furthermore, NTs were not observed in the proximity of the window or pointed electrodes.

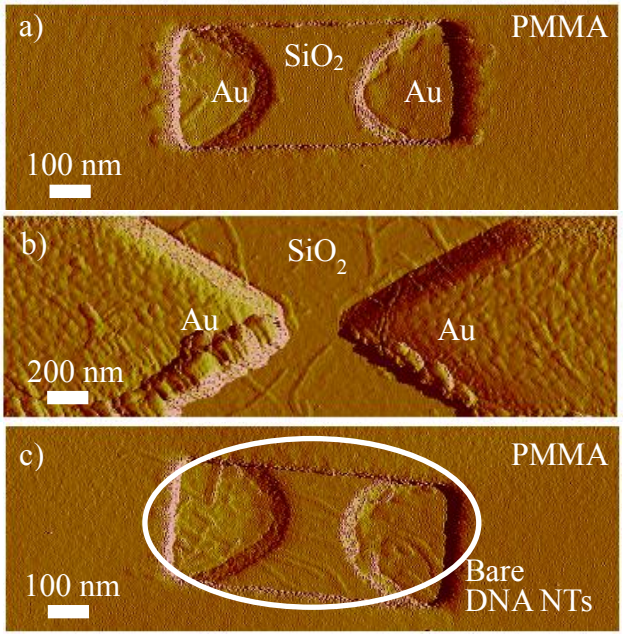

Figure 4.2 (a) AFM amplitude image of a pointed electrode structure with PMMA window. ~0.83 nM bare DNA NTs that were end thiolated were deposited using direct deposition via pipetting. NTs were not observed bridging the electrodes. (b) AFM amplitude image of a pointed electrode structure without a PMMA window. ~ 1 nM bare DNA NTs were deposited using direct deposition via pipetting and NTs were observed near the pointed electrodes but not bridging the electrodes. (c) AFM amplitude image of a pointed electrode structure with PMMA window. ~ 3.7 nM bare DNA NTs that were end thiolated were deposited using direct deposition via pipetting and NTs were observed bridging the electrodes. The concentration of the DNA NTs being deposited is important because at higher concentrations successful bridging of electrodes is likely to occur. All three pointed electrode structures are the same design but not the same structure.

Additionally, increasing the bare NT concentration to ~1 nM and removing the PMMA window did not result in successful NT bridging, however bare NTs were observed near the pointed electrodes as shown in Figure 4.2b. Only when the concentration of bare DNA NTs was increased to ~3.7 nM were NTs observed bridging the pointed electrodes as shown in Figure 4.2c. Achieving a higher concentration of the bare DNA NTs is not difficult, but attaining a AuNP functionalized DNA NT concentration of over 1 nM is difficult and problematic due to the filtration steps required, thus the low concentration of the AuNP DNA NTs was a limiting factor. An alternative approach to increase the probability of NT bridging was required, which led to a redesign towards an improved electrode structure. The new Au electrode structure was designed to increase the probability of DNA NT bridging with the design constraint requiring the use of the low NT concentration in mind.

Due to the difficulty in increasing the NT concentration above 1 nM, another approach was required to increase the probability of NT bridging. The parallel Au electrode structure offered such an opportunity. The parallel Au electrode structure was designed to increase the probability of DNA NTs bridging without increasing the concentration of the NTs by replacing the original, pointed electrodes with long, parallel finger electrodes and removing the PMMA-defined window region. The idea for the parallel electrode structure came from an analysis of AFM images of AuNP DNA NTs deposited on mica. The deposition (pipetting) of the NTs is performed in the absence of any field gradient (e.g., chemical potential, temperature, pressure, electric field, directional flow, etc.), hence, the deposition established a random distribution of NTs across the surface. A random distribution of DNA origami NTs within the small gap area

defined by the PMMA window on the pointed electrodes structure structures constrained the deposition of the NTs into a small, specific area. To increase the bridging area, a parallel electrode design was devised. To demonstrate the concept of increased bridging area, Figure 4.3 shows the design of the Au parallel electrodes overlaid on an AFM image of a ~1 nM solution of DNA origami NTs. The number of observed bridging NT events is at least two.

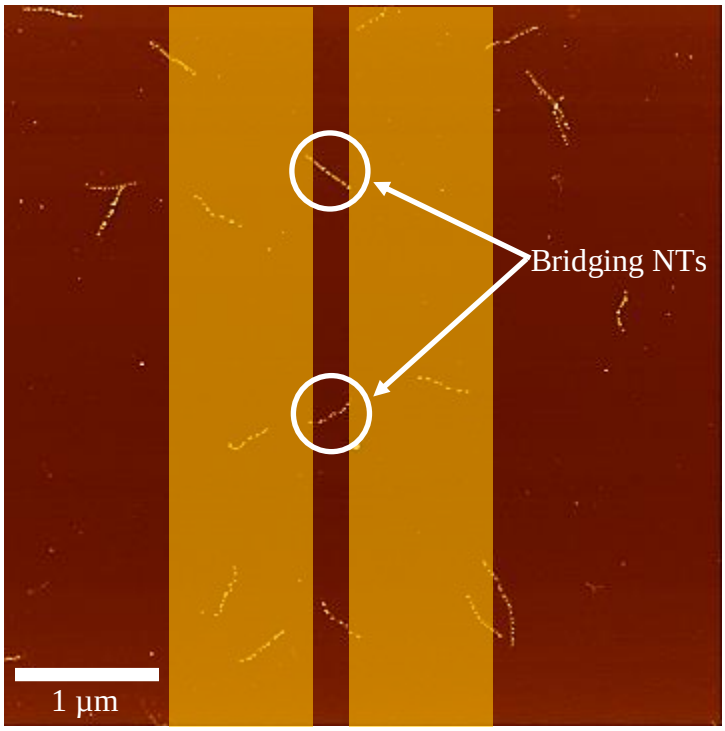

Figure 4.3 Proposed 1 µm wide Au electrodes separated by a 250 nm gap (gold rectangles in the image) overlaid on a 5 µm × 5 µm AFM height image of 29-site AuNP DNA origami NTs on mica. In the proposed image of the electrode design, there are two different points where NTs are bridging the electrodes.

An estimate for the number of NTs available for bridging under ideal conditions is given by:

$$\text{Number of NTs} = \text{Gap Area} \times \text{NT Concentration} \times \text{Avogadro's \#} \times \left(\frac{\text{Amount of NT solution Deposited in Liters}}{\text{Area of Deposition}}\right) \quad (4.1)$$

Assuming a gap area of 250 nm x 250 nm for the pointed electrodes structure, a NT concentration of 1 nM, 36 µL of NT and buffer solution deposited, and a diameter of 8 mm for the droplet that is deposited, it was calculated that the number of NTs available for bridging is ~27. If a gap area of 250 nm x 15 µm is used for the parallel electrode structure and the same parameters as before, the calculated number of NTs available for bridging increases to ~1617. Although it is a rough and simplified calculation, it does reveal how the parallel electrode structure design provides about two orders of magnitude more NTs for bridging. Hence, the calculation indicates that such a design will most likely increase the probability for DNA NT bridging of the electrodes without having to increase the concentration of the AuNP DNA NT solution.

To incorporate the parallel electrodes into the previous pointed electrode design, the only change required was to remove the pointed electrodes and add the parallel electrodes. Hence, the same contact pads and electrode extensions leading to the parallel finger electrodes from the first design with the pointed electrodes were retained as shown in Figure 4.1b, saving time on the redesign. The parallel electrode structure originally incorporated two 60 µm long finger electrodes with a 350 nm gap between the electrodes, but the finger electrodes were reduced to 15 µm long to reduce the time required to AFM image the entire length of the electrodes. Additionally, the gap was reduced from 350 nm to 250 nm to augment the probability of a NT bridging the electrodes considering that NT bridging normal to the electrodes would have a very low probability. The electrode

extensions connecting the contact pads to the parallel finger electrodes were removed on the final structure and the contact pads were also reduced from 50 µm x 50 µm to 40 µm x 40 µm to decrease on EBL write times. The final design of the parallel finger electrode structure is shown in Figure 4.1c.

Depositions of the AuNP functionalized DNA NTs performed on the parallel electrode structure (see 2.2.6 DNA Origami Nanotube Deposition) demonstrated successful bridging of DNA origami NTs as shown in Figure 3.6. The depositions were performed without having to increase the concentration of the AuNP DNA NT solution as predicted. The ability to bridge the electrodes with the NTs without having to increase the concentration of the NT solution was an important accomplishment because electrical characterization of the AuNP DNA NTs (Figure 3.6d, Figure 3.8, and Figure 3.9) was now possible, an important requirement for this thesis.

4.2 Conductivity of Bare DNA Origami Nanotubes and Viability as a Suitable Substrate

One of the goals of this thesis was to evaluate if DNA origami NTs are a suitable substrate (i.e., nanobreadboard) for the fabrication of nanoscale electronic and optoelectronic devices by site-specific functionalization of NPs. It was hypothesized that bare DNA origami NTs were nonconductive substrates for AuNP attachment or Au seeding and would demonstrate conductive behavior only after Au functionalization and subsequent Au enhancement. It is hypothetically expected that only after Au enhancement of either the AuNP functionalized NTs or Au seeded NTs would conductivity be observed. Hence, two control experiments were required to assess this hypothesis. The control experiments were to establish that both bare NTs and bare NTs exposed to the Au enhancement solution were not conductive. The reasoning for the latter control experiment was to ensure that Au enhancement solution would not result in Au plating of the bare NT, which could lead to observed conductivity.

The hypothesis for the first control experiment was borne out as electrical measurements indicated the bare NTs were not conductive, as shown in Figure 3.5d. Similarly, electrical characterization of the bare DNA NTs, post Au enhancement, did not reveal evidence of conductivity, also shown in Figure 3.5d. These results demonstrate that the DNA origami NTs are a suitable insulative substrate, within the design constraints, for the fabrication of nanoscale electronic and optoelectronic devices by site-specific functionalization of NPs. Others have also shown that additional DNA origami structures, such as triangles and rectangles, were also nonconductive [63-65], supporting

the hypothesis that DNA origami structures could be a suitable insulative substrate (nanobreadboard) for the fabrication of electronic and optoelectric devices.

4.3 Au Functionalized DNA Origami Nanotubes and Electrical Conductivity

To further examine whether or not DNA origami NTs are a suitable substrate for the fabrication of nanoscale electronic and optoelectronic devices by site-specific functionalization of NPs, the DNA NTs were functionalized with AuNPs and Au clusters to assess their electrical behavior. It was also theorized that by increasing the size of the AuNPs or Au clusters, an electrically conductive Au fictionalized DNA NT could be fabricated. DC-IV measurements were performed on Au functionalized DNA NTs before and after Au enhancement to determine if the conductivity changes upon increasing the size of the AuNPs and seeds.

DNA origami NTs functionalized with AuNPs were not conductive before Au enhancement as shown in Figure 3.6d and the Au seeded DNA NTs were also not conductive prior to Au enhancement as shown in Figure 3.12. Both devices exhibited similar, measured resistances in the 10^{12} Ω range. The AuNP DNA NTs were not expected to conduct because of the large spacing between the AuNPs on the NTs. Figure 4.4a-e are AFM height images and counts of the AuNPs spanning the gap between the electrodes. If all 29-sites were occupied by 5 nm diameter AuNPs, approximately 16 AuNPs would be expected to span the gap. From examining Figure 4.4a-e, there are only 4-8 AuNPs spanning the gap on the devices, resulting in larger inter-particle spacing of ~62.5 nm to ~31.25 nm. As a result, electrical conduction through tunneling is highly unlikely, which was substantiated by simulations by Thompson *et al.* [74] performed using the Energy Band Diagram Program developed by Boise State University [75, 76]. The simulations show that a voltage of ~120 V is required for Fowler-Nordheim tunneling of electrons to occur on a 29-site DNA origami NT functionalized with 5 nm

diameter AuNPs, which is over 6 orders of magnitude greater than the -1mV to 1mV sweeps used in this study. As for the Au seeded DNA NTs, from the AFM height image shown in Figure 3.2c, the Au clusters appear to be covering the surface of the NT. However, the IV data implies the Au coverage alone is not sufficient enough to create a conductive NT.

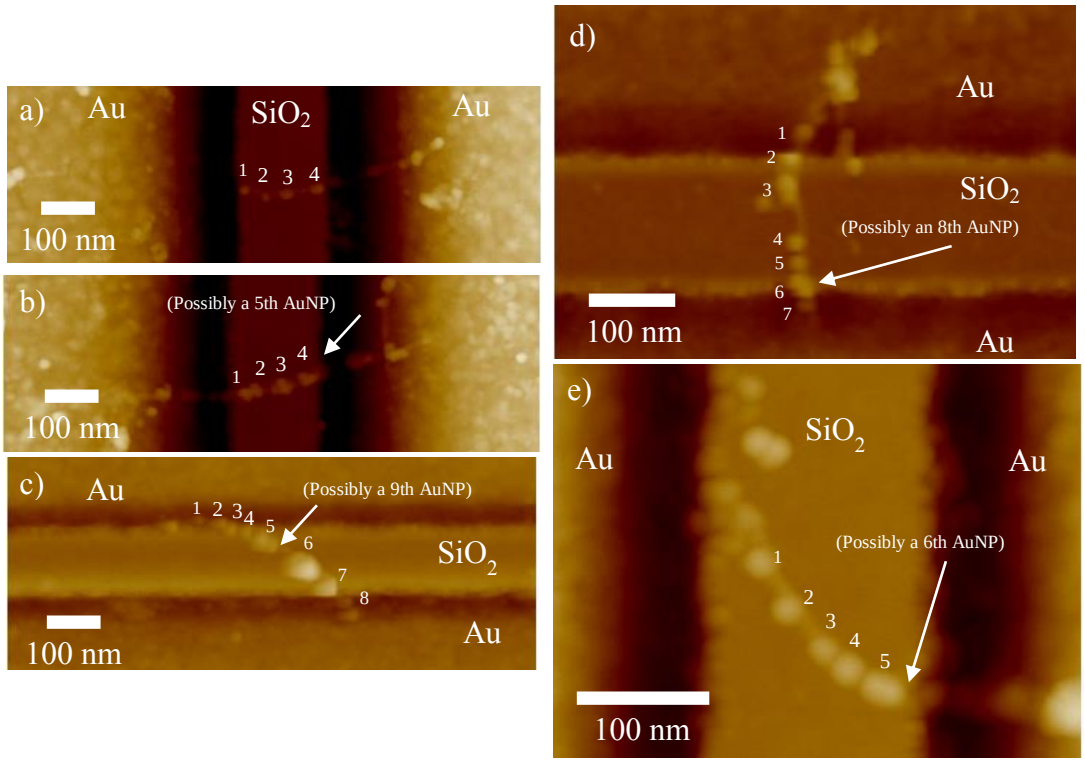

Figure 4.4 AFM height images of AuNP DNA NT depositions (not Au enhanced) onto electrodes that were used to count the approximate number of AuNPs spanning the gap between the electrodes. Images b-e include arrows pointing towards possible AuNPs that were not easily delineated. (a) Device 1: 4 AuNPs span the gap between the electrodes (b) Device 2: 4 AuNPs spanning the gap (c) Device 3: 8 AuNPs spanning the gap (d) Device 4: 7 AuNPs spanning the gaps (e) Device 5: 5 AuNPs spanning the gap

Au enhancement solution was used to increase the size of the AuNPs and Au seeds on the DNA origami NTs for two reasons: (1) to enhance the electrical conductivity

of the Au functionalized DNA NTs, and (2) to assess if the conductivity of DNA NTs functionalized with AuNPs or seeded with Au clusters would change depending on the size of the AuNPs or Au clusters. Electrical conductivity was observed with the 15 minute Au enhanced AuNP DNA NTs (Figure 3.8) and with the Au seeded DNA NTs after 7 and 9 minutes of Au enhancement (Figure 3.12 and Figure 3.14).

The IV data indicates that the Au enhancement solution can be used to increase the size of the AuNPs or Au clusters and enhance the electrical conductivity of the Au functionalized DNA NTs. The dimensions of the AuNP DNA NTs increased after 15 minutes of Au enhancement was applied as shown in Table 3.2, however, it is difficult to distinguish the individual AuNPs as they have merged together as shown by the AFM height images before in Figure 3.6c and after 15 minutes of Au enhancement in Figure 3.7b. Though it can be shown that an electrically conductive NT can be fabricated from the attachment of AuNPs on the DNA NTs and after Au enhancement is performed, it is difficult to determine if the conduction can be controlled through the size of the AuNPs due to the merging of the AuNPs. Preliminary Au enhancements of the AuNP DNA NTs involved 10 minute enhancements, but reliable DC-IV measurements were difficult to achieve because of the durability of the contact pads on the early electrode structures. However, a single AuNP DNA NT that was Au enhanced for 10 minutes was electrically characterized and a resistance of ~60 kΩ was measured. Figure 4.5 shows the resistance of the AuNP DNA NTs for different Au enhancement times. Following the red line connecting the data points, the resistance decreases with increased Au enhancement time. The standard deviation for 15 minutes of Au enhancement is represented in the blue error bar. The standard deviation was not calculated for 10 minutes of Au enhancement as

there was only one measurement and before Au enhancement the measured resistance of TΩ is at the limit of the equipment. To fully assess if the conduction can be controlled through the size of the AuNPs, experiments with shorter Au enhancement times would need to be performed where the growth of the AuNPs could clearly be observed and DC-IV measurements performed.

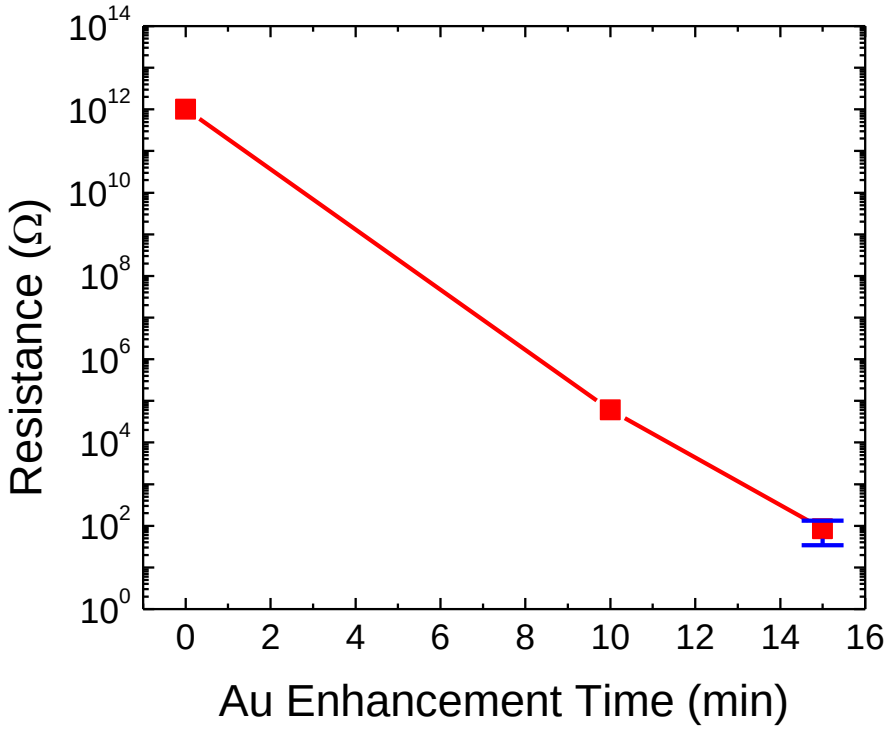

Figure 4.5 AuNP functionalized DNA origami NT resistance as a function of Au enhancement time. As the Au enhancement time was increased, a decrease in the resistance was observed. The red line connecting the data points is included to help show the decrease in resistance. The standard deviation for 15 minutes of Au enhancement is represented by the blue error bar. Reliable DC-IV measurements were difficult to obtain on 10 minute Au enhanced AuNP DNA NTs because the contact pads on the early electrode structures were not durable enough, but one recorded resistance was included in the plot for a comparison to the 15 minutes of Au enhancement.

Au seeded DNA NTs were also Au enhanced for 5, 7, and 9 total minutes to evaluate if the conductivity can be increased and controlled by changing the particle size

using Au enhancement. Two devices were investigated, each with a different number of bridging NTs. The two devices contained 2 and 3 bridging Au seeded NTs, respectively. Both devices S2 and S3 showed electrical conductivity with decreasing resistance after each enhancement as shown in Figure 4.6. Following the lines connecting the data points, the resistance decreases as Au enhancement time is increased.

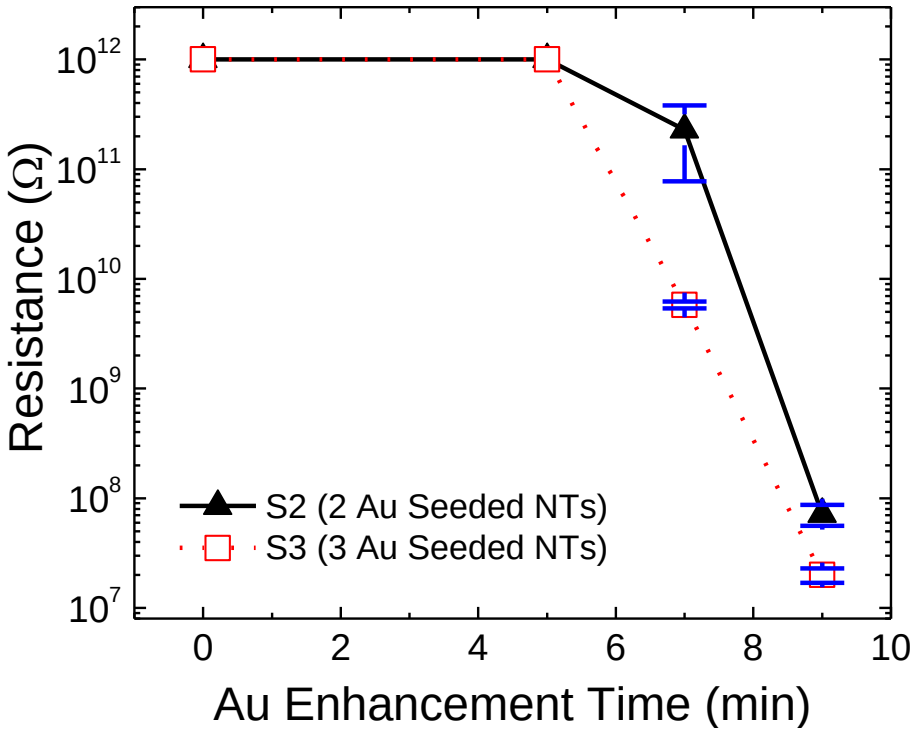

Figure 4.6 Au seeded NT devices S2 and S3's resistance as a function of Au enhancement time. As the total amount of Au enhancement time is increased, the resistance decreases for both devices as shown by the lines connecting the data points. Standard deviation is represented in the blue error bars. The standard deviation was not calculated before Au enhancement and for 5 minutes because the resistance is in the TΩ and at the limit of the equipment.

The Au clusters appear to be less merged together than the AuNPs after the different Au enhancement times as shown in Figure 3.11. The decrease in resistance between the different Au enhancement times of the Au seeded DNA NTs indicates it may

be possible to increase the conductivity of a Au functionalized DNA NT by adjusting the particle size using the Au enhancement method. However, further experiments with more devices would need to be performed to gather a larger sample size and confirm this.

The AuNP DNA NTs were compared to the Au seeded DNA NTs to determine if either design is more advantageous in controlling the electrical behavior of the Au functionalized DNA origami NTs. The DNA NTs functionalized with AuNPs is aligned with the hypothesis of this thesis because of the adjustable number of site-specific, binding sites. However, the attachment yield of the AuNPs on the 29-site AuNP DNA NTs only a modest ~55-58% (3.1 DNA Origami Nanotubes), resulting in a larger than expected spacing between the adjacent AuNPs. On the other hand, synthesis steps required to functionalize the DNA origami NTs using the Au seeding solution is simpler. AuNP functionalization of the DNA origami NTs requires multiple steps such as annealing and filtering using gel electrophoresis (2.2.1 DNA Origami Nanotubes). Using the positively charged Au cluster solution to seed the NTs does provide a simpler method to cover the entire DNA origami NT in Au. However, it does not allow one to functionalize the DNA NT at specific sites. Controlling the conductivity would then rely on increasing the particle size using Au enhancement solution rather than the number of AuNPs attached. Both the AuNP functionalized and Au seeded DNA NTs were not conductive before Au enhancement solution was applied, so currently neither method can create a conductive structure as synthesized.

Neither the Au seeded nor the AuNP decorated NT design showed control of the Au growth using Au enhancement solution as both designs resulted in non-uniform growth of the AuNPs and Au seeds as shown in the AFM images Figure 3.3, Figure 3.7,

Figure 3.10, Figure 3.11, and Figure 3.13. As expected, the AuNP DNA NTs Au enhanced for 15 minutes were larger than the Au seeded DNA NTs Au enhanced for 9 minutes because the initial AuNP diameter is 5 nm while the initial Au cluster diameter is 1.4 nm. The average height, average width perpendicular to the NT (referred to as perpendicular width), and average length of the Au enhanced NTs spanning the gap (i.e., not the total length of the NT) of the device with 3 Au seeded DNA NTs Au enhanced for 9 minutes were 37.8 nm, 43.5 nm, and 115.2 nm, respectively. The average height, average perpendicular width, and average length of the Au enhanced NTs of the 5 devices examined of the 15 minute Au enhanced AuNP DNA NTs were 68.4 nm, 82.2 nm, and 120.2 nm, respectively. The heights for both Au enhanced DNA NT designs were close to the characterized Au enhancement heights of the AuNPs shown in Table 3.1. Additional experiments are required to compare the measured resistance of the 15 minute Au enhancement of the AuNP DNA NTs to determine if similar or lower resistances can be achieved. The experiments might include enhancing the Au seeded DNA NTs for 15 minutes.

In conclusion, electrically conductive Au functionalized DNA NTs were fabricated and electrically characterized with resistances lower than what others have reported for similar structures [44]. It was found that neither Au functionalized NT design proved to be more advantageous in terms of controlling the conductivity. The Au enhancement of both the AuNPs and the Au seeds was non-uniform. Additional experiments would need to be performed to examine if the electrical conductivity could be controlled through the size of the AuNPs or Au seeds using Au enhancement solution.

4.3.1 Possible Causes for Large Difference in Resistances for AuNP DNA Nanotubes

Initial DC-IV measurements of the AuNP DNA NTs after Au enhancement resulted in devices 1 and 2 with resistances in the MΩ and devices 3-5 with resistances of ~60 Ω. One possible reason for the large difference in resistance could be due to the nucleotides from the DNA linker strands on the AuNPs. As Au enhancement is performed, the nucleotides can still be present on the AuNPs as they are being enlarged, as shown in the schematic in Figure 4.7. The nucleotides could act as an insulation barrier, impeding the conductivity of the Au enhanced AuNP DNA NT. Others have hypothesized that some causes could be electron scattering from grain boundaries, impurities, or defects in the Au enhanced NTs [33, 40, 44].

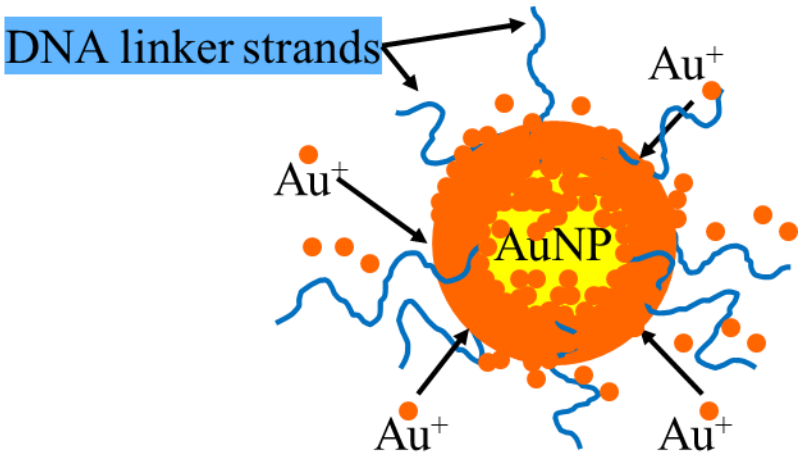

Figure 4.7 Schematic of the DNA linker strands acting as an insulation barrier as Au enhancement is performed. The DNA linker strands are still present as the AuNP is enhanced.

Another possibility was that the AuNPs were not merging together because of the non-uniform growth of the AuNPs after Au enhancement. Due to the observed non-uniform growth of the AuNPs after applying the Au enhancement solution as shown in

Figure 3.3, it is difficult to predict the manner in which the AuNPs or Au clusters will be enhanced. In Figure 3.3b, the SEM image shows visible boundaries between the AuNPs that may indicate the AuNPs are not completely merged together. Possibly a combination of the nucleotides creating an insulation barrier and the non-uniform growth of the Au during Au enhancement may be the reason why some of the structures have higher resistances than others after Au enhancement.

4.3.2 Decreased Resistances for Au DNA Origami Nanotubes Following SEM Imaging

SEM images of the Au enhanced Au functionalized DNA NTs bridging the electrode structures, shown in Figure 4.8, were obtained to measure the perpendicular widths of the Au enhanced NTs as listed in Table 3.2.

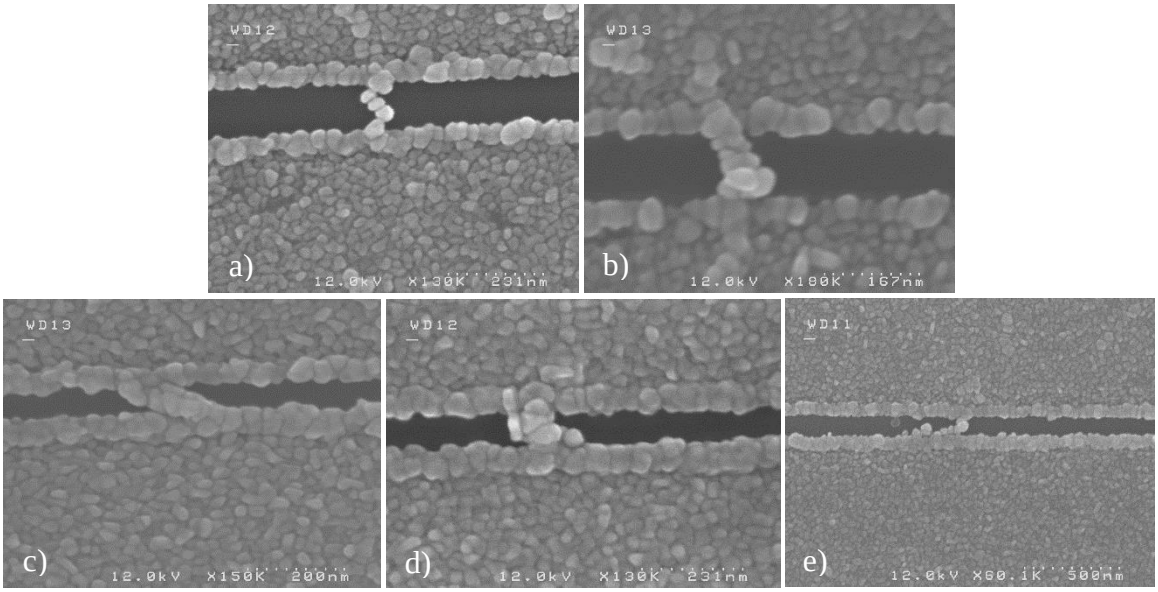

Figure 4.8 SEM images of single AuNP DNA origami NTs Au enhanced for 15 minutes (a) Device 1 (b) Device 2 (c) Device 3 (d) Device 4 (e) Device 5.

The five devices with AuNP DNA NTs bridging the electrodes were electrically characterized before and after SEM imaging to determine if damage had occurred to the

NTs during imaging. Prior to SEM imaging, the resistances of device 1 and device 2 were in the MΩ range. After SEM imaging, the resistance of device 1 and device 2 decreased to ~170 Ω and ~82 Ω, respectively. Device 3 and device 5 resistances' remained at ~60 Ω, however the resistance of device 4 decreased from to 64 Ω ~48 Ω. Based on the decreased resistances, the resistivity of each device was calculated and remained greater in value compared to expected value of bulk Au as shown in Table 4.1 (see APPENDIX C). Following SEM imaging, the resistance of S3 also decreased from ~22 MΩ to ~9 MΩ. In the following paragraphs, possible reasons to explain the decrease in resistance following SEM imaging are discussed.

Table 4.1 Calculated Bulk Resistivity for Au enhanced AuNP DNA NTs

Device	Calculated resistance ($\rho = 2.44 \times 10^{-8}$ Ω·m)	Measured resistance before SEM imaging	Calculated bulk resistivity ρ before SEM imaging	Measured resistance after SEM imaging	Calculated bulk resistivity after SEM imaging
1	1.65 Ω	~ 8 MΩ	1.18×10^{-1} Ω·m	~ 170 Ω	2.51×10^{-6} Ω·m
2	0.79 Ω	~ 1 MΩ	3.08×10^{-2} Ω·m	~ 82 Ω	2.53×10^{-6} Ω·m
3	0.43 Ω	~ 64 Ω	3.64×10^{-6} Ω·m	~ 60 Ω	3.42×10^{-6} Ω·m
4	0.29 Ω	~ 64 Ω	5.24×10^{-6} Ω·m	~ 48 Ω	3.93×10^{-6} Ω·m
5	0.73 Ω	~ 60 Ω	2×10^{-6} Ω·m	~ 60 Ω	2×10^{-6} Ω·m

One possible idea for the decrease in the resistance of the devices following SEM imaging may be due to deposition of conductive contamination such as carbon during SEM imaging [77, 78]. It has been shown by de Pablo *et al.* that low energy electron bombardment can induce contamination and reduce the resistivity of λ-DNA [78]. Perhaps any exposed DNA on the Au functionalized DNA NTs after Au enhancement (i.e., linker strands on the AuNPs or the NT itself) are being modified or contaminated.

Others have used electron beam exposure to improve electrical measurement performance of different nanowires. Richter *et al.* used the deposition of electron-beam-induced carbon lines over the end of Pd nanowires where the nanowires contacted the Au electrodes to mechanically fix the nanowires and lower the contact resistance of the Pd nanowire [55]. The Pd nanowires initially exhibited a resistance below 5 kΩ before mechanical stabilization and the resistance was measured below 1 kΩ after mechanical stabilization [55]. Bachtold *et al.* used an SEM to selectively expose areas of carbon NTs that contacted Au electrodes with an electron beam to decrease the contact resistance [77]. The resistance of the carbon NTs after exposure ranged from 0.35 kΩ – 2.6 kΩ. Bachtold *et al.* performed several experiments to determine the cause of the decrease in resistance. Some of the hypothesis included that the contacts between the Au electrode and the carbon NT were being modified, that a film of amorphous carbon was deposited during exposure, or that the NT itself was affected after exposure. It was determined that the exposure only affected the contact between the carbon NT and Au electrode, reducing the contact resistance [77].

To assess the effects of carbon deposition during SEM imaging, a control study was performed in which SEM was used to deposit a carbon resistor between electrode tips of a pointed electrode structure. The pointed electrodes were exposed using the SEM for an extended amount of time (~15 min) in an attempt to deposit enough carbon to bridge the electrodes, though the exact time and parameters of the SEM were not recorded. The resistance of the resulting carbon film, deemed a carbon resistor, was extracted from a linear fit of the I-V data shown in Figure 4.9 in the green line. The resistance of the carbon resistor was just over 6GΩ.

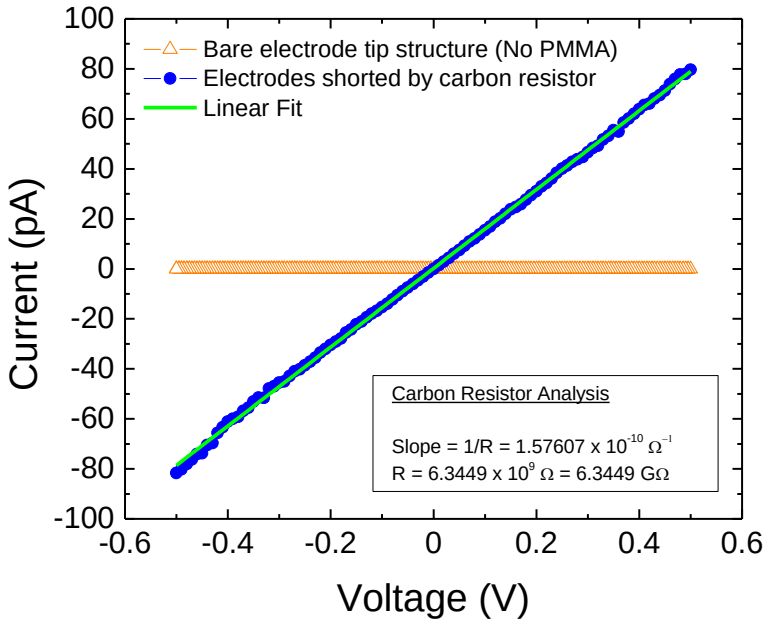

Figure 4.9 DC-IV of an electrode structure before and after deposition of a carbon resistor in which the resistance of the carbon resistor (~6 GΩ) was extracted via a linear fit.

Because the resistance of the carbon resistor is at least 7 orders of magnitude greater than the resistances of the devices exposed by SEM as shown in Figure 4.10, it is highly unlikely that carbon contamination is the reason for the substantial decrease in the resistance of the tested devices. Furthermore, the contact resistance was expected to be already low for devices 1-5 and S3 because, following the Au enhancement, the NT and Au electrodes appear to have merged together (i.e., Figure 3.7b and c). For this reason, it is unlikely that a decrease in contact resistance was the reason for the observed change in resistance for the NTs subsequent to SEM imaging.

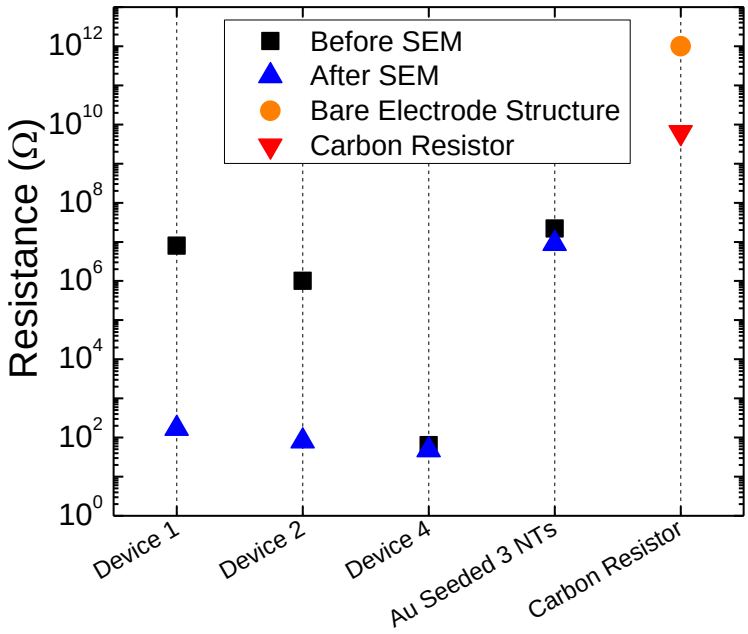

Figure 4.10 Comparison of the measured resistance of the Carbon Resistor to the Au functionalized NTs before and after SEM imaging. The Carbon Resistor's resistance is at least 7 orders of magnitude larger than the Au functionalized NTs, and it is unlikely that carbon contamination is the reason for the decreased resistance after SEM imaging.

Another possible reason for the subsequent decrease in resistance could be due to the electron beam vaporizing the nucleotides (analogous to electron beam evaporation) or possibly annealing of the Au on the structures from the electron beam during imaging [79]. However, the different parameters of the SEM such as the area scanned, scan rate, beam current, and time scanned were all varied between each device in this study, so it is difficult to determine if the NTs were annealed. Nevertheless, future experiments are required if it is deemed necessary to further investigate the SEM-initiated resistance decrease in some of the devices.

CHAPTER FIVE: CONCLUSION

DNA origami NTs functionalized with and without AuNPs were synthesized and DC-IV electrically characterized. DNA origami NTs were also seeded with positively charged Au clusters and electrically characterized. Bare DNA NTs without Au were not conductive indicating that the bare DNA NTs are a suitable "nanobreadboard." The AuNP functionalized DNA NTs were not conductive either, but following a 15 minute exposure to Au enhancement solution, the AuNP DNA NTs exhibited linear, ohmic conductivity, and resistances ranging from ~60 Ω to ~8 MΩ. Possible reasons for the larger difference in the observed resistances for some devices include a combination of nucleotides acting as an insulation barrier and the non-uniform growth of the Au during Au enhancement. DNA NTs seeded with positively charged Au clusters were also conductive after Au enhancement with linear, ohmic behavior. The resistance is in the MΩ range after 9 minutes of Au enhancement. SEM imaging induced a decrease in resistances for several Au enhanced AuNP functionalized DNA NTs with final resistances ranging from ~48 Ω to ~170 Ω. A decrease in resistance after SEM imaging was also observed in one of the Au seeded NT devices. Possible hypotheses for the decreased resistance after SEM imaging include the electron beam vaporizing nucleotides or annealing the Au enhanced NTs. These findings indicate that by functionalizing the DNA origami nanotube with AuNPs or Au clusters and using Au enhancement, an electrically conductive structure can be fabricated. DNA origami NTs functionalized with

Au with tunable conductivity may have applications in variety of electronic and optoelectronic devices such as a nanowires or sensor.

5.1 Future Work

Possible areas of improving and augmenting this study include:

1. Performing electrical characterization of Au enhanced DNA origami NTs functionalized with differing number of sites such as 5, 9, and 15 sites for AuNPs to examine how varying the number of attached AuNPs affect the conductivity.
2. Au enhancement over a broader range of enhancement time performed on the NTs to analyze the growth of the AuNPs.
3. An in-depth study of the Au enhancement process and how the DNA oligonucleotides used to functionalize the AuNPs are affected during Au enhancement.
4. Increasing the yield of AuNP attachment on the 29-site AuNP DNA NT devices in order to synthesize a more conductive structure.
5. Functionalize the DNA origami NTs designed with different number of sites with different diameter sizes of AuNPs.
6. Perform experiments determine the cause for the reduced resistance of the NTs after SEM imaging.
7. Perform a growth study of the Au seeded structures to determine if the growth rate and behavior is similar to the AuNP DNA NTs.

8. Continue additional Au enhancements of the Au seeded NTs after 9 minutes and perform DC-IV measurements to determine if the resistance decreases after continued enhancements.
9. Electrically characterize a single Au seeded NT.
10. Use Au seeding to metalize other DNA origami structures and electrically characterize.
11. A heterogeneous DNA Origami NT structure - a combination of AuNPs and other NPs such as QDs could be synthesized and electrically characterized to create nanostructures with different conductivities and applications.

REFERENCES

[1] N. C. Seeman, "DNA in a material world," *Nature,* vol. 421, pp. 427-431, 2003.

[2] P. W. K. Rothemund, "Folding DNA to create nanoscale shapes and patterns," *Nature,* vol. 440, pp. 297-302, Mar 2006.

[3] L. Qian, *et al.*, "Analogic China map constructed by DNA," *Chinese Science Bulletin,* vol. 51, pp. 2973-2976, 2006.

[4] S. M. Douglas, *et al.*, "DNA-nanotube-induced alignment of membrane proteins for NMR structure determination," *Proceedings of the National Academy of Sciences,* vol. 104, pp. 6644-6648, April 17, 2007 2007.

[5] E. S. Andersen, *et al.*, "DNA Origami Design of Dolphin-Shaped Structures with Flexible Tails," *ACS Nano,* vol. 2, pp. 1213-1218, 2008/06/01 2008.

[6] J. Sharma, *et al.*, "Toward Reliable Gold Nanoparticle Patterning On Self-Assembled DNA Nanoscaffold," *Journal of the American Chemical Society,* vol. 130, pp. 7820-7821, 2008/06/01 2008.

[7] Y. Ke, *et al.*, "Scaffolded DNA Origami of a DNA Tetrahedron Molecular Container," *Nano Letters,* vol. 9, pp. 2445-2447, 2009/06/10 2009.

[8] Y. Ke, *et al.*, "Multilayer DNA Origami Packed on a Square Lattice," *Journal of the American Chemical Society,* vol. 131, pp. 15903-15908, 2009/11/04 2009.

[9] M. Endo, *et al.*, "DNA Prism Structures Constructed by Folding of Multiple Rectangular Arms," *Journal of the American Chemical Society,* vol. 131, pp. 15570-15571, 2009/11/04 2009.

[10] S. M. Douglas, *et al.*, "Rapid prototyping of 3D DNA-origami shapes with caDNAno," *Nucleic Acids Research,* June 16, 2009 2009.

[11] S. M. Douglas, *et al.*, "Self-assembly of DNA into nanoscale three-dimensional shapes," *Nature,* vol. 459, pp. 414-418, 2009.

[12] E. S. Andersen, *et al.*, "Self-assembly of a nanoscale DNA box with a controllable lid," *Nature,* vol. 459, pp. 73-76, 2009.

[13] A. Kuzuya and M. Komiyama, "Design and construction of a box-shaped 3D-DNA origami," *Chemical Communications,* pp. 4182-4184, 2009.

[14] H. Dietz, *et al.*, "Folding DNA into Twisted and Curved Nanoscale Shapes," *Science,* vol. 325, pp. 725-730, August 7, 2009 2009.

[15] A. Kuzuya and M. Komiyama, "DNA origami: Fold, stick, and beyond," *Nanoscale,* vol. 2, pp. 310-322, 2010.

[16] D. Han, *et al.*, "DNA Origami with Complex Curvatures in Three-Dimensional Space," *Science,* vol. 332, pp. 342-346, April 15, 2011 2011.

[17] H. Bui, *et al.*, "Programmable Periodicity of Quantum Dot Arrays with DNA Origami Nanotubes," *Nano Letters,* vol. 10, pp. 3367-3372, 2010.

[18] C. Onodera, "Structural DNA Origami: Engineering Supermolecular Self-Assembly For Nanodevice Fabrication," Master of Science in Materials Science

and Engineering, College of Engineering: Materials Science and Engineering, Boise State University, Boise, 2012.

[19] F. Mathieu, *et al.*, "Six-Helix Bundles Designed from DNA," *Nano Letters,* vol. 5, pp. 661-665, 2005/04/01 2005.

[20] E. Braun, *et al.*, "DNA-templated assembly and electrode attachment of a conducting silver wire," *Nature,* vol. 391, pp. 775-778, 1998.

[21] S. J. Park, *et al.*, "Array-based electrical detection of DNA with nanoparticle probes," *Science,* vol. 295, pp. 1503-1506, Feb 2002.

[22] H. Yan, *et al.*, "DNA-Templated Self-Assembly of Protein Arrays and Highly Conductive Nanowires," *Science,* vol. 301, pp. 1882-1884, September 26, 2003 2003.

[23] D. Liu, *et al.*, "DNA nanotubes self-assembled from triple-crossover tiles as templates for conductive nanowires," *Proceedings of the National Academy of Sciences of the United States of America,* vol. 101, pp. 717-722, January 20, 2004 2004.

[24] S. H. Park, *et al.*, "Three-Helix Bundle DNA Tiles Self-Assemble into 2D Lattice or 1D Templates for Silver Nanowires," *Nano Letters,* vol. 5, pp. 693-696, 2005/04/01 2005.

[25] H. A. Becerril, *et al.*, "DNA-Templated Three-Branched Nanostructures for Nanoelectronic Devices," *Journal of the American Chemical Society,* vol. 127, pp. 2828-2829, 2005/03/01 2005.

[26] S. H. Park, *et al.*, "Optimized fabrication and electrical analysis of silver nanowires templated on DNA molecules," *Applied Physics Letters,* vol. 89, pp. 033901-3, 2006.

[27] M. Fischler, *et al.*, "Formation of Bimetallic Ag–Au Nanowires by Metallization of Artificial DNA Duplexes," *Small,* vol. 3, pp. 1049-1055, 2007.

[28] M. Pilo-Pais, *et al.*, "Connecting the Nanodots: Programmable Nanofabrication of Fused Metal Shapes on DNA Templates," *Nano Letters,* vol. 11, pp. 3489-3492, 2011/08/10 2011.

[29] S. H. Park, *et al.*, "Electronic nanostructures templated on self-assembled DNA scaffolds," *Nanotechnology,* vol. 15, p. S525, 2004.

[30] F. Patolsky, *et al.*, "Au-Nanoparticle Nanowires Based on DNA and Polylysine Templates," *Angewandte Chemie,* vol. 114, pp. 2429-2433, 2002.

[31] K. Keren, *et al.*, "Sequence-Specific Molecular Lithography on Single DNA Molecules," *Science,* vol. 297, pp. 72-75, July 5, 2002 2002.

[32] O. Harnack, *et al.*, "Tris(hydroxymethyl)phosphine-Capped Gold Particles Templated by DNA as Nanowire Precursors," *Nano Letters,* vol. 2, pp. 919-923, 2002/09/01 2002.

[33] A. Ongaro, *et al.*, "DNA-Templated Assembly of Conducting Gold Nanowires between Gold Electrodes on a Silicon Oxide Substrate," *Chemistry of Materials,* vol. 17, pp. 1959-1964, 2005/04/01 2005.

[34] T. Nishinaka, *et al.*, "Conductive Metal Nanowires Templated by the Nucleoprotein Filaments, Complex of DNA and RecA Protein," *Journal of the American Chemical Society,* vol. 127, pp. 8120-8125, 2005/06/01 2005.

[35] D. Aherne, *et al.*, "Diameter-dependent evolution of failure current density of highly conducting DNA-templated gold nanowires," *Nanotechnology,* vol. 18, p. 125205, 2007.
[36] J. Lee, *et al.*, "DNA Assisted Assembly of Multisegmented Nanowires," *Electroanalysis,* vol. 19, pp. 2287-2293, 2007.
[37] R. Mohammadzadegan, *et al.*, "DNA-templated gold nanowires," *Physica E: Low-dimensional Systems and Nanostructures,* vol. 41, pp. 142-145, 2008.
[38] S. Kundu and H. Liang, "Microwave Synthesis of Electrically Conductive Gold Nanowires on DNA Scaffolds," *Langmuir,* vol. 24, pp. 9668-9674, 2008/09/02 2008.
[39] A. Swami, *et al.*, "Phase Transfer of Gold Metallized DNA," *Journal of Cluster Science,* vol. 20, pp. 281-290, 2009.
[40] Q. Gu, *et al.*, "Fabrication of nickel and gold nanowires by controlled electrodeposition on deoxyribonucleic acid molecules," *Journal of Physics D: Applied Physics,* vol. 42, p. 015303, 2009.
[41] Z. Zhao, *et al.*, "Encapsulation of Gold Nanoparticles in a DNA Origami Cage," *Angewandte Chemie International Edition,* vol. 50, pp. 2041-2044, 2011.
[42] R. Schreiber, *et al.*, "DNA Origami-Templated Growth of Arbitrarily Shaped Metal Nanoparticles," *Small,* vol. 7, pp. 1795-1799, 2011.
[43] J. Liu, *et al.*, "Metallization of Branched DNA Origami for Nanoelectronic Circuit Fabrication," *ACS Nano,* vol. 5, pp. 2240-2247, 2011/03/22 2011.
[44] A. C. Pearson, *et al.*, "DNA Origami Metallized Site Specifically to Form Electrically Conductive Nanowires," *The Journal of Physical Chemistry B,* 2012.
[45] Q. Gu, *et al.*, "Cobalt metallization of DNA: toward magnetic nanowires," *Nanotechnology,* vol. 16, p. 1358, 2005.
[46] Q. Gu and D. T. Haynie, "Palladium nanoparticle-controlled growth of magnetic cobalt nanowires on DNA templates," *Materials Letters,* vol. 62, pp. 3047-3050, 2008.
[47] C. F. Monson and A. T. Woolley, "DNA-Templated Construction of Copper Nanowires," *Nano Letters,* vol. 3, pp. 359-363, 2003/03/01 2003.
[48] H. Kudo and M. Fujihira, "DNA-templated copper nanowire fabrication by a two-step process involving electroless metallization," *Nanotechnology, IEEE Transactions on,* vol. 5, pp. 90-92, 2006.
[49] Q. Gu, *et al.*, "DNA-templated fabrication of nickel nanocluster chains," *Physica E: Low-dimensional Systems and Nanostructures,* vol. 33, pp. 92-98, 2006.
[50] H. A. Becerril, *et al.*, "DNA-Templated Nickel Nanostructures and Protein Assemblies," *Langmuir,* vol. 22, pp. 10140-10144, 2006/11/01 2006.
[51] W. E. Ford, *et al.*, "Platinated DNA as Precursors to Templated Chains of Metal Nanoparticles," *Advanced Materials,* vol. 13, pp. 1793-1797, 2001.
[52] M. Mertig, *et al.*, "DNA as a Selective Metallization Template," *Nano Letters,* vol. 2, pp. 841-844, 2002/08/01 2002.
[53] R. Seidel, *et al.*, "Synthesis of Platinum Cluster Chains on DNA Templates: Conditions for a Template-Controlled Cluster Growth," *The Journal of Physical Chemistry B,* vol. 108, pp. 10801-10811, 2004/07/01 2004.
[54] J. Richter, *et al.*, "Nanoscale Palladium Metallization of DNA," *Advanced Materials,* vol. 12, pp. 507-510, 2000.

[55] J. Richter, *et al.*, "Construction of highly conductive nanowires on a DNA template," *Applied Physics Letters,* vol. 78, pp. 536-538, 2001.
[56] J. Richter, *et al.*, "Low-temperature resistance of DNA-templated nanowires," *Applied Physics A: Materials Science & Processing,* vol. 74, pp. 725-728, 2002.
[57] Z. Deng and C. Mao, "DNA-Templated Fabrication of 1D Parallel and 2D Crossed Metallic Nanowire Arrays," *Nano Letters,* vol. 3, pp. 1545-1548, 2003/11/01 2003.
[58] H. Liu, *et al.*, "Approaching The Limit: Can One DNA Oligonucleotide Assemble into Large Nanostructures?," *Angewandte Chemie International Edition,* vol. 45, pp. 1942-1945, 2006.
[59] K. Nguyen, *et al.*, "Synthesis of Thin and Highly Conductive DNA-Based Palladium Nanowires," *Advanced Materials,* vol. 20, pp. 1099-1104, 2008.
[60] S. Kundu, *et al.*, "Photoinduced Formation of Electrically Conductive Thin Palladium Nanowires on DNA Scaffolds," *Langmuir,* vol. 25, pp. 10146-10152, 2009/09/01 2009.
[61] Y. Geng, *et al.*, "Rapid metallization of lambda DNA and DNA origami using a Pd seeding method," *Journal of Materials Chemistry,* vol. 21, pp. 12126-12131, 2011.
[62] A. Kuzyk, *et al.*, "Dielectrophoretic Trapping of DNA Origami," *Small,* vol. 4, pp. 447-450, 2008.
[63] E. P. Bellido and et al., "Current–voltage–temperature characteristics of DNA origami," *Nanotechnology,* vol. 20, p. 175102, 2009.
[64] A. D. Bobadilla, *et al.*, "DNA origami impedance measurement at room temperature," *Journal of Chemical Physics,* vol. 130, May 2009.
[65] V. Linko, *et al.*, "Characterization of the Conductance Mechanisms of DNA Origami by AC Impedance Spectroscopy," *Small,* vol. 5, pp. 2382-2386, Nov 2009.
[66] V. Linko, *et al.*, "Defined-size DNA triple crossover construct for molecular electronics: modification, positioning and conductance properties," *Nanotechnology,* vol. 22, Jul 2011.
[67] R. J. Kershner, *et al.*, "Placement and orientation of individual DNA shapes on lithographically patterned surfaces," *Nat Nano,* vol. 4, pp. 557-561, 2009.
[68] B. Ding, *et al.*, "Interconnecting Gold Islands with DNA Origami Nanotubes," *Nano Letters,* vol. 10, pp. 5065-5069, 2010.
[69] N. F. Mott and E. A. Davis, *Electronic Processes in Non-Crystalline Materials,* 2nd ed. Oxford: Clarendon-Press, 1979.
[70] M. Frei. (2011, January 6). *Centrifugation Basics*. Available: http://www.sigmaaldrich.com/technical-documents/articles/biofiles/centrifugation-basics.html
[71] *GoldEnhance - EM*. Available: http://www.nanoprobes.com/pdf/Inf2113.pdf
[72] R. Sherman, *et al.*, "Surface cleaning with the carbon dioxide snow jet," *Journal of Vacuum Science & Technology A: Vacuum, Surfaces, and Films,* vol. 12, pp. 1876-1881, 1994.
[73] *Nanoindenting and Nanoscratching*. Available: http://www.bruker.com/products/surface-analysis/atomic-force-

microscopy/modes/modes-techniques/specialized-modes/nanoindent-nanoscratch.html

[74] R. J. Thompson, *et al.*, "New Applications of the Boise State Band Diagram Program," presented at the IEEE International Integrated Reliability Workshop, Fallen Leaf Lake, CA, 2011.

[75] R. G. Southwick and W. B. Knowlton, "Stacked dual-oxide MOS energy band diagram visual representation program (IRW student paper)," *Device and Materials Reliability, IEEE Transactions on,* vol. 6, pp. 136-145, 2006.

[76] R. G. Southwick, *et al.*, "An Interactive Simulation Tool for Complex Multilayer Dielectric Devices," *Device and Materials Reliability, IEEE Transactions on,* vol. 11, pp. 236-243, 2011.

[77] A. Bachtold, *et al.*, "Contacting carbon nanotubes selectively with low-ohmic contacts for four-probe electric measurements," *Applied Physics Letters,* vol. 73, pp. 274-276, 1998.

[78] P. J. de Pablo, *et al.*, "Absence of dc-Conductivity in λ-DNA," *Physical Review Letters,* vol. 85, pp. 4992-4995, 2000.

[79] R. F. Egerton, *et al.*, "Radiation damage in the TEM and SEM," *Micron,* vol. 35, pp. 399-409., 2004.

APPENDIX A

General Electrode Structure Fabrication Process

General processing procedure and specifications for fabricating the electrode structures.

Wafer

- Si wafers ordered from University Wafer
  - Diameter: 100 mm
  - Orientation: (100)
  - Resistivity: 0-100 Ohm
  - Doping Type: p-type
  - Thickness: 500 µm
  - Polish: One-Side
  - Requests: 500 nm thermal oxide

PMMA spin-on Procedure

- 60% PMMA (450 PMMA) solution
  - Spin-on at 3000 RPM for 45 seconds with 5 second ramp period before to deposit PMMA
  - Bake for ~10 min at 180˚C
  - Yields ~100-125 nm thick PMMA

Electron Beam Lithography Procedure

- Prepared wafer diced into ~1 cm × 1 cm pieces for EBL
- LEO 1430-VP Scanning Electron Microscope
  - 30 kV beam
  - ~8-12 pA beam current
  - Faraday cup and gold reference used to optimize beam
  - Electrode structure pattern written/exposed in PMMA using NPGS (Nanometer Pattern Generation System)

Development Procedure

- Developed in MIBK:IPA 1:3 solution (~100 mL) for 1 minute (30 seconds agitated, 30 seconds rest)
- Etch in Buffered Oxide Etchant for 40 seconds agitated

Sputter Deposition Procedure

- Sputtered in custom-built Kyle R. See Physical Vapor Deposition tool
- Vacuum chamber pressure taken down to at least 5 x10^{-6} Torr, then pumped Ar into chamber at 25.5 sccm to induce plasma
- Cr plasma gun run at 50W for 5:30 (min:sec) to obtain ~30 nm of Cr

- Au plasma gun run afterwards at 50W for 7:30 (min:sec) to obtain ~70 nm of Au

Post-Process Cleaning Procedure

- Wafer sonicated in acetone (~100 mL) and AIM washed (acetone, isopropanol, and methanol)
- Dried with ultrahigh-pure nitrogen gas
- Additional cleaning performed: snow clean (CO_2 clean)

APPENDIX B

AFM Procedures

General procedure to perform AFM imaging and nanomanipulation of DNA NTs using AFM.

B.1 Tapping Mode with Tip Tuned to the Right of the Tuning Curve

The tapping mode with the tip tuned to the right of the tuning curve (attractive) is sometimes called “non-contact” mode. However, this name is somewhat of a misnomer as contact is made, albeit very soft contact. Using this technique, the synthesized NTs and resulting depositions of the NTs were imaged and verified using the AFM (Bruker Dimension Icon FastScan AFM and FastScan-A tips). This technique was chosen over other AFM imaging techniques because of the speed and quality of the images obtained and to avoid damaging the samples. The “non-contact” mode was introduced to the research group recently from Bruker representatives, and a considerable amount of time was invested to optimize the technique for imaging the DNA NTs on the electrode structures. Others in the group have continued to use this technique for capturing images of other DNA origami structures. Images were captured using a tapping mode where the tip was tuned to the right of the tuning curve to place the system in an attractive mode/non-contact mode:

1) After starting the Nanoscope software, select “Tapping Mode” under Experiment Category, select “Tapping Mode in Air” under Experiment group, and select “Tapping Mode in Air” under Experiment.
2) In the the Setup, tune the tip normally for tapping mode. Change the “Target Amplitude” to 200 mV and the “Peak Offset” should be 5%. Select “Autotune” and wait for the system to finish tuning. The “Drive Amplitude” should be between ~20-70 mV after performing the tune. If

not, reposition the tip in the tip holder or select a new tip. The "Amplitude Setpoint" should be set to ~170-180 mV so that it lies beneath the tip of the peak of the tuning curve.

3) Check Parameters: Change the "Scan Size" to 0 nm and reduce the "Scan Rate" to 2 Hz.

4) From the Menu, select "Microscope" → "Engage Settings" and set the "Engage Setpoint" to "1" (without the quotes) and the "Engage Mode" to "Standard."

5) After engaging onto the surface, select the "Tune" icon (Figure B.1) and enter "50 nm" (without the quotes) for the desired tune height.

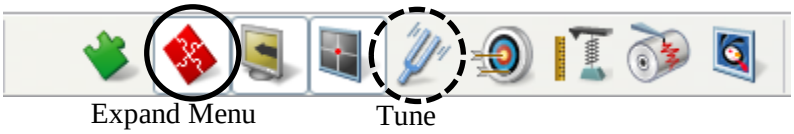

Figure B.1 Expand Menu and Tune Icons.

6) In the Cantilever Tune prompt, change the "Drive Amplitude" until 2 nm of tip deflection is achieved (~10 mV Drive Amplitude). This is indicated when the tuning curve's peak is at 2 nm on the Y-axis (Figure B.2).

7) After the tip deflection is set at 2 nm, change the "Amplitude Setpoint" until the purple line at the top of the peak (~40 mV to 50 mV).

8) In the Cursor Mode menu, select "Offset" and move the "Drive Frequency" red/green vertical line until it is sufficiently to the right of the peak of the tuning curve. When the green/red vertical line is at the desired frequency, select "Execute" to set the "Drive Frequency."

9) Click “Exit” to leave the Cantilever Tune.

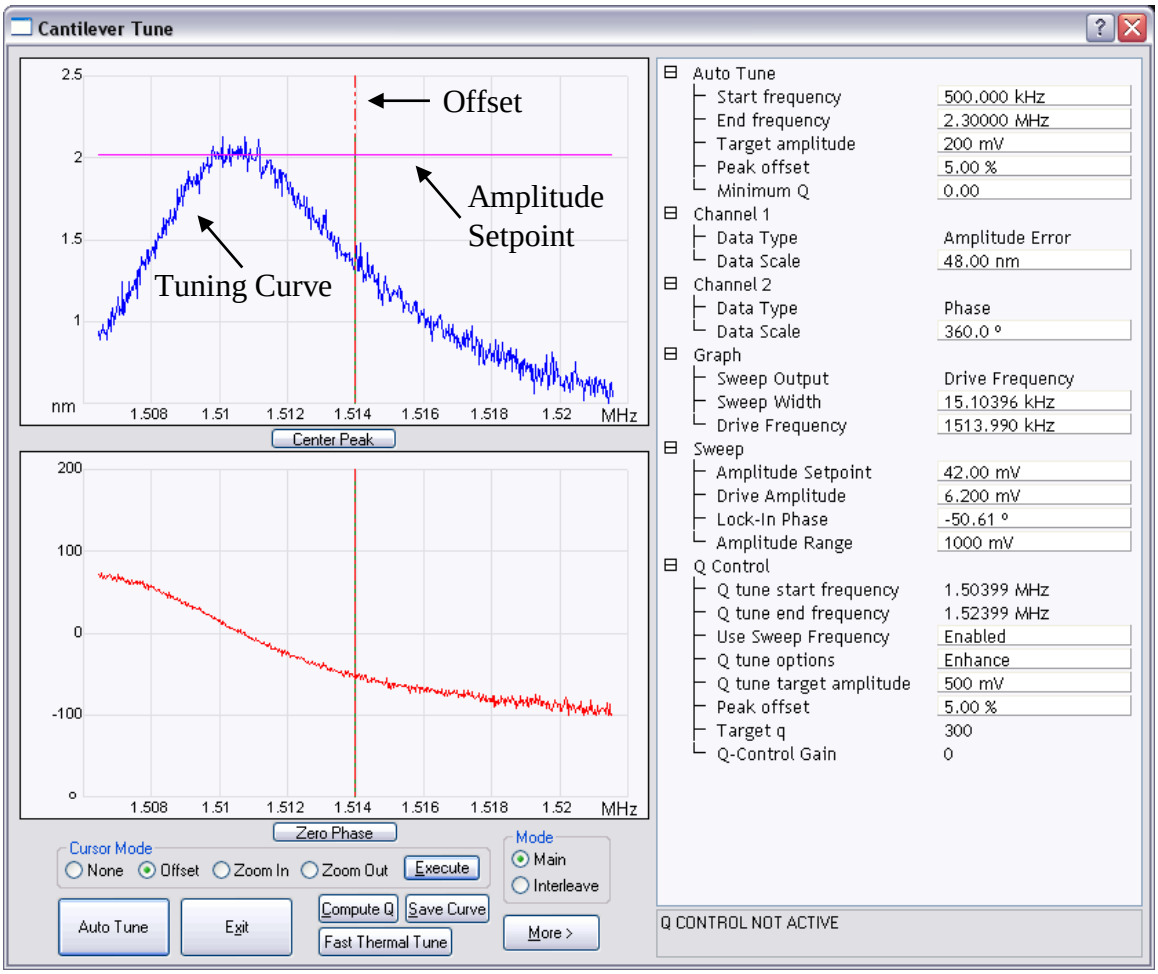

Figure B.2 Tuning curve (blue) with the tip tuned for 2 nm of deflection and to the right of the peak. The Amplitude Setpoint (purple line) is set to a voltage so that it is at the peak of the tuning curve.

10) After tuning the tip, the tip will not track on the surface and the image will be lost. To begin the process to get the tip to track on the surface again, select the “Expanded Mode” icon (Figure B.1) and change the “Lock-in BW” to 50 kHz.

11) Start decreasing the Amplitude Setpoint in small increments (~2 mV) until tip begins tracking the surface again.
12) Change the "Scan Size" to ~500 nm and continue decreasing the Amplitude Setpoint until the desired tracking is achieved. Additionally, the Integral Gain and Proportional Gain can be adjusted to help with the tracking. For imaging of the NTs on mica, lower gains were used such as 1 for the Integral Gain and 5 for the Proportional Gain, but with the parallel electrode structures a minimum of 2 for the Integral Gain and 10 for the proportional Gain was used. The user will need to experiment with the two Gains and determine the best Gains for the sample.
13) The user can now set the desired settings (Scan Rate, Samples/Line, etc.) for capturing an image.

B.2 NanoMan – Bruker's Nanomanipulation Mode

The removal of debris and unwanted NTs in the gap between the electrode structures was accomplished using NanoMan, an AFM technique created by Bruker that allows the user to manipulate nanoscale-sized objects. The NanoMan tab that is used is the Path tab that allows the user to draw straight lines of how the tip should move for subsequent execution (Figure B.3).

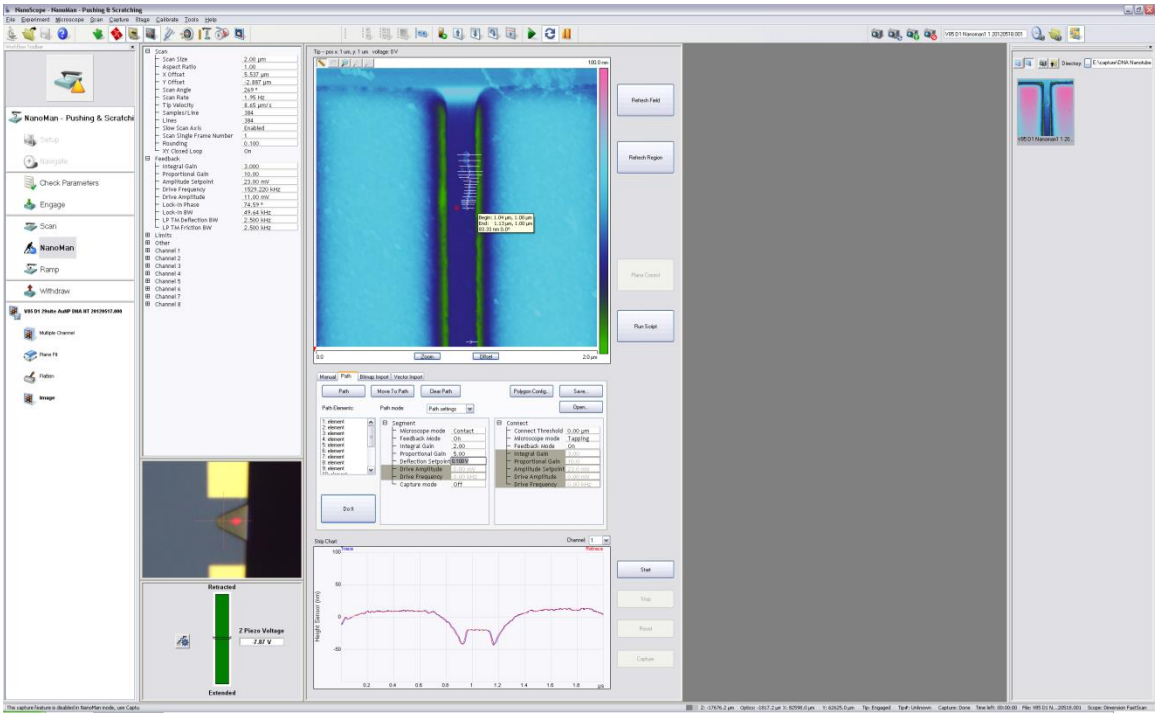

Figure B.3 NanoMan interface for pushing and scratching.

NanoMan was performed using the Bruker Dimension FastScan AFM, FastScan-A tip, and imaging mode described in General procedure to perform AFM imaging and nanomanipulation of DNA NTs using AFM.

B.1 Tapping Mode with Tip Tuned to the Right of the Tuning Curve.

1) From the list of experiments in NanoScope, choose “Other SPM” under Experiment Category, and then select “Nanomanipulation” under Experiment group, and finally select “Pushing and Scratching” under Experiment.
2) Run the Setup and tune the tip for desired imaging procedure (i.e., Tapping or Non-contact).
3) Use the Navigate option to move to the desired location on sample.

4) From the Menu, select “Microscope” → “Engage Settings” and set the “Engage Setpoint” to “1” (without the quotes) and the “Engage Mode” to “Standard.”
5) Check Parameters and set the required Scan Size, Scan Rate, etc.
6) Engage onto the surface of the sample.
7) After the AFM is imaging, make sure the appropriate height scale for the image has been chosen, because once NanoMan mode is chosen, the image’s height scale cannot be changed.
8) Click on the “NanoMan” option located between “Scan” and “Ramp.”
9) The interface for NanoMan (Figure B.3) will now be the active window. Select the tab that says “Path.” In this mode, the AFM will scan the area first, pause and wait for the user to input their desired moves by drawing lines or “paths” onto the scanned area, and then execute the movements.
10) Click on “Refresh Field” to take a scan of the area and wait until it has completed. When the scan has finished, an image can be saved using the “Capture Now” (CTRL + N) command.
11) The user can now begin to draw lines or “paths” onto the scanned image of where the tip should move. Lines are drawn by left clicking at the start point and while continuing to hold down the left click, and then dragging the end point of the line to the desired position and releasing the left click. An arrow will indicate the direction the tip will move. Any sequence of lines can be drawn, but order is important because the software will move the tip in the sequence the lines have been drawn. For example, in Figure

B.4, the software will start at the top of the sequence of lines and move down until it has finished all the movement in attempt to push away the NT. Also, if the lines are drawn end to end, the software will connect the ends of the lines and create one long push or scratch.

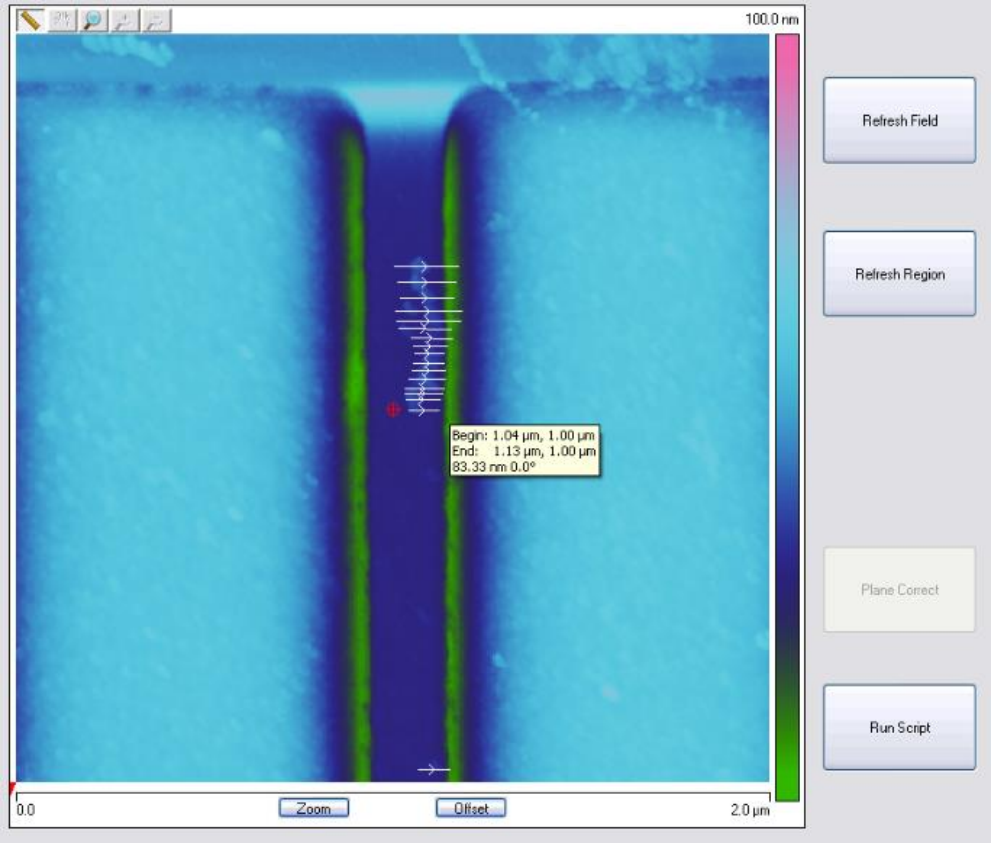

Figure B.4 Lines or "paths" can be drawn on the scanned image of where the user wants the tip to move.

12) In the “Path” tab, the “Path Mode” should be set to “Path setting.” Under the “Segment” tree, the following settings should be set (Figure B.5):

Microscope Mode: Contact
Feedback Mode: On
Integral Gain: 2
Proportional Gain: 5
Deflection Setpoint: 0.1 V
Capture mode: Off

These setting are the default settings except for the Deflection Setpoint. Once the user has become more familiar with NanoMan, the user may want to try different Gains.

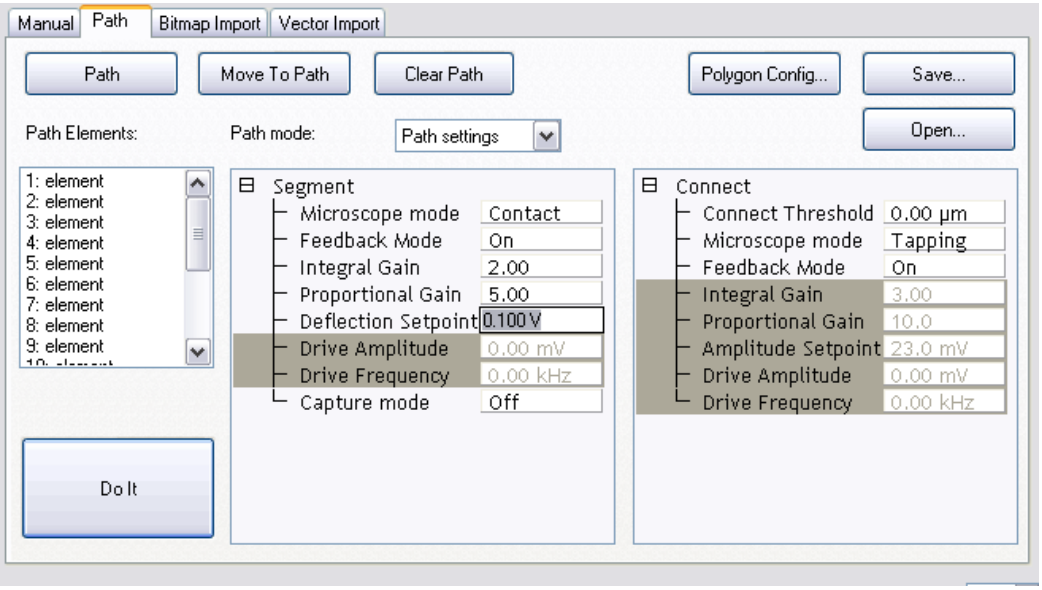

Figure B.5 Beginning Path segment settings for NanoMan.

13) After the Segment parameters have been set, click on the “Do It” button to move the tip. The tip will then go through the sequence of lines until the

movements are done. If an error message appears that says the "Z is out of range" (Figure B.6), increase the "Deflection Setpoint" in 0.1 V steps until the error message disappears.

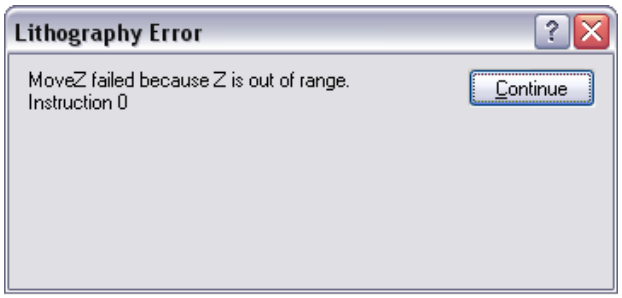

Figure B.6 Z is out of range error. If this message appears, increase the Deflection Setpoint.

14) After the sequence of paths has been executed, click Refresh Field to rescan the entire image. After the scan has finished, the user can either move the already drawn paths to a new location, delete lines by right clicking on lines and selecting "Delete," or draw additional lines. The lines/paths can be executed again by clicking "Do It."

15) If only a small area of the scan needs to be refreshed, the "Refresh Region" button can be used. After clicking the "Refresh Region" button, the user can draw a box around the area that needs to be rescanned and only that area will be refreshed. The already drawn lines can be adjusted, moved, or deleted, but additional lines/paths cannot be drawn if "Refresh Region" is used. The lines/paths can be executed again by clicking "Do It."

16) If the object has not moved, try increasing the “Deflection Setpoint” in small increments or extending out the line/path to see if that improves the movement.
17) The user can repeat NanoMan until the object has been moved. The scanned area can then be changed using the Zoom or Offset options to move to a new location.
18) To exit NanoMan, select “Withdraw” to withdraw the tip and end scanning or select “Scan” to return to normal imaging.

APPENDIX C

Expected Resistances of 15 minute Au Enhanced AuNP DNA NTs

Calculations for the expected resistances for the 15 minute Au Enhanced AuNP DNA NTs.

Expected Resistance Calculations for the 15 minute Au Enhanced AuNP DNA NTs

A comparison of the measured resistances with the expected resistance for the Au enhanced AuNP DNA NTs was performed as a first order approximation to examine if the expected resistance could provide insight to why there was a large difference in the measured resistance. It was considered that the enhanced AuNPs along the DNA NT is a uniform Au wire and the Au wire has an average height, width, and length. The Au enhanced AuNP dimensions (Table 3.2) were used to calculate an expected resistance using the expression:

$$R = \rho \frac{L}{A} \qquad \text{(C.1)}$$

where ρ is the bulk resistivity of Au (2.44×10^{-8} Ω·m), *L* is the length of the Au enhanced AuNP DNA NT (not the possible conduction path as discussed earlier), and *A* is the area of the NT (height × perpendicular width). The calculated resistances are presented in Table C.1. The measured resistance and calculated resistances do not match as the calculated resistances are significantly less than the measured resistances. However, the NTs on devices 1 and 2 were expected to have the largest resistances as there are fewer NPs spanning the gap and smaller heights and perpendicular widths. Furthermore, according to the calculations, devices 1 and 2 did have the largest measured resistances, but were not calculated to have as large a difference in resistance as observed in the measured resistance (5 orders of magnitude difference). The calculations do provide a

lower bound for the lowest, expected resistances for the devices measured, but the calculated resistances are below the measured internal resistance of ~3 Ω for the Keithley 4200 SCS. The measured resistances are greater than the internal resistance of the Keithley 4200 SCS, so the measured resistances are deemed credible. The resistivities of the Au DNA Origami NTs were also calculated using the measured resistances and calculated to be higher than the bulk resistivity of Au. The higher resistivity could be due to several possibilities including impurities or grain boundaries present after Au enhancement [33, 40, 44].

Table C.1 Calculated resistance and resistivity of Au enhanced, AuNP DNA NTs

Device	# of AuNP spanning the gap	Measured resistance before SEM imaging	Calculated resistance ($\rho = 2.44 \times 10^{-8}$ Ω·m)	Calculated bulk resistivity ρ
1	4	~ 8 MΩ	1.65 Ω	1.18×10^{-1} Ω·m
2	5	~ 1 MΩ	0.79 Ω	3.08×10^{-2} Ω·m
3	6-7	~ 64 Ω	0.43 Ω	3.64×10^{-6} Ω·m
4	7-8	~ 64 Ω	0.29 Ω	5.24×10^{-6} Ω·m
5	5-6	~ 60 Ω	0.73 Ω	2×10^{-6} Ω·m